Models of Charged Domain Walls

A Thesis Submitted to the Committee on Graduate Studies
in Partial Fulfillment of the Requirements for the
Degree of Master of Science in the Faculty of Arts and Science.

Trent University
Peterborough, Ontario, Canada

Materials Science M.Sc. Graduate Program
January 2024

Abstract

Models of Charged Domain Walls

Carson Carroll

There is a 'universal' picture of a charged domain wall (CDW) in theoretical work, often depicted as residing in an infinite thickness film, charge neutral, and with no bias voltage applied. However, in experiment CDWs are shown with none of these assumptions. CDWs are produced in thin or ultra-thin films, the CDW is not charge neutral, and a bias voltage is being applied. We look to go beyond these assumptions. It was shown that a positively charged domain wall (DW) moves against an external electric field which is not expected. The free electron density was also shown to determine the DW displacement amount. When the film thickness is lowered (ultra-thin film) we get a negatively charged DW which still moves against an external electric field, which agrees with experiment of a CDW in a ultra-thin film. This suggests the charge on the DW does not determine displacement direction.

Keywords: Charged domain wall, ferroelectricity, ferroelectric material.

Acknowledgments

A sincere thank you to Prof. Bill Atkinson. It was a tough journey but I could always count on his patience and guidance.

Thank you to my committee members Prof. Aaron Slepkov and Prof. Matthew Kaye for their advice and constructive feedback.

I would like to thank the entire Department of Physics and Astronomy at Trent University for their support of students and providing a productive environment to learn in.

Contents

List of Figures

List of Tables

Chapter 1

Introduction

1.1 Overview

Ferroelectric materials form domains, which are regions of differing polarization orientation. The plane separating the domains, the domain wall (DW), is an important aspect when considering the electrical, electromechanical, and optical properties of ferroelectrics. The domain wall has previously just been considered a border between the domains. However, in recent theoretical and experimental research the inner properties of domain walls have sparked interest.

Charged domain walls (CDW) specifically, have motivated a lot of research because they possess bound charge. The bound charge attracts free electrons or holes which accumulate at the domain wall and screen the bound charge. The free electrons or holes act as a conducting channel along the domain wall. Ferroelectrics for the most part are insulating, and the domains remain insulating even with a charged domain wall acting as a conductive channel. Domain walls are movable through application of an external electric field. Ultimately, ferroelectric materials with charged domain walls can be thought of as insulating materials with a movable conductive channel. Writable electronics are a big motivation for research into charged domain walls. The idea behind writable electronics is that charged domain walls can act as nano-wires or planes, which can be configured by applying an external electric field to make nano-circuitry.

The surface bound charge, σ_b, at the domain wall can be described by

$$\sigma_b = (\overline{P_1} - \overline{P_2}) \cdot \hat{n_1} \tag{1.1}$$

where $\hat{n_1}$ is the vector normal to the domain wall and $\overline{P_1}$ and $\overline{P_2}$ are the polarization vectors of each domain on either side of the domain wall. Positively charged domain walls require screening from free electrons to remain stable and for the polarization to persist. The free electrons can come from defects in the material such as oxygen vacancies, and from doping, for example [1–3]. For perfect screening the free electrons or holes, given as a 2-D electron density n_{2d}, would need to create a surface charge at the domain wall equal and opposite to σ_b, which is unlikely. The unscreened bound charge produces an electric field, known as a depolarizing field, acting in opposite direction of the polarization, effectively reducing it. In order to theoretically model a charged domain wall we need to capture the physics happening at the domain wall.

A full theoretical model requires solving coupled equations for polarization, electron density, and electric field. These equations are solved numerically, which is computationally intensive. Sturman *et al.* have proposed a set of equations that suggest a universal form for charged domain walls [4]. The approximations made to arrive at this set of equations speed up the computation time tremendously. The goal of the thesis is to see how the approximations hold up, go beyond the limitations of Sturman's approximations and assumptions, and to understand the physics of charged domain walls for systems of real physical interest.

1.2 Ferroelectricity

A ferroelectric material has a spontaneous polarization that is switchable by an external electric field [5]. Spontaneous polarization in this case comes from an electric dipole moment within each crystal unit cell. The dipole moment arises from a shift in the ionic positions due to a phase transition that breaks inversion symmetry below a critical temperature. One region of the unit cell is therefore positively charged and another region is negatively charged, and the polarization points from the negative region towards the positive region, in the direction of the positive bound charge. This is the key concept of polarization and

ferroelectrics. In an ideal ferroelectric material, all the unit cells that make up the material are polarized and they align in the same direction, giving rise to a uniform polarization.

Common ferroelectrics have a perovskite crystal structure, which is the structure of interest in this thesis. Some examples of perovskite ferroelectrics include $BaTiO_3$, $Pb(Zr,Ti)O_3$, and $LiTaO_3$. Perovskites have an ABO_3 structure, where A and B are positively charged cations and O are oxygen ions (in an octahedral formation). This can be seen in Figure 1.1. In the perovskite crystal structure, the dipole moment comes from the positively charged ions and negatively charged O ions shifting in opposite directions.

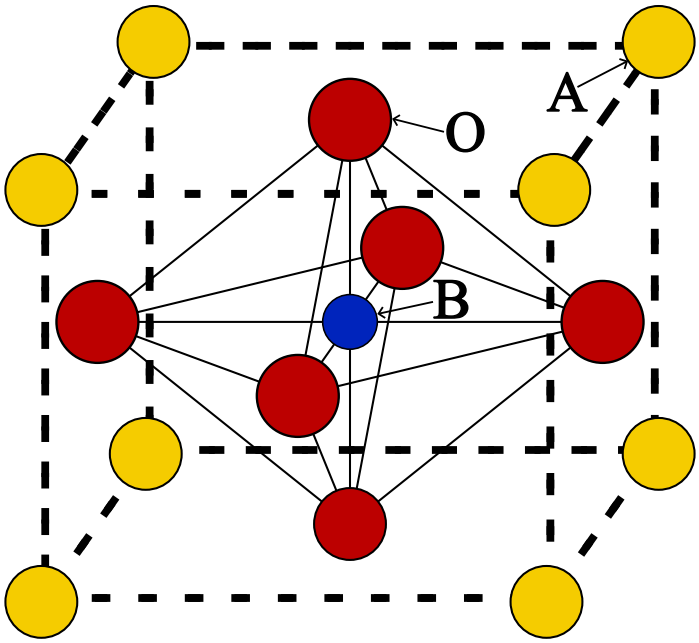

Figure 1.1: Cubic ABO_3 perovskite structure. A and B are positively charged cations. O are oxygen ions in an octahedral formation.

1.2.1 Applications

Ferroelectrics have gathered interest for their potential next generation use as non-volatile memory [6,7]. Commercial ferroelectric RAM (FRAM) devices do exist, but are considered niche products or are used alongside other memory devices [5]. The polarization orientation can be flipped by applying an electric field and the voltage required to make that flip can be measured. The value of the voltage reveals the state of the material. This would be considered a read function in the memory. One would then have to re-apply the voltage

in the opposite direction to return the material to its original state, or write state. This application utilizes the orientation and magnitude of the polarization in each domain for the read/write process. The main interest in CDW is their use for next generation circuitry, which utilizes the DW itself rather than the polarization in the domain. CDW applications use the high conductivity of the CDW as nano-wires or planes, with the ability to move the conducting channel, the DW, by applying an external electric field [8, 9].

1.2.2 Domain Formation

Why do domains form?

In practice, ferroelectric materials do not generally have a uniform polarization throughout the material. A uniform polarization would lead to surface charges, which is energetically unfavorable as the surface charges generate an electric field that stores energy. The system wants to lower its energy and to do so it creates domains within the material. Domains are regions within the material that have polarization pointing in different directions from neighbouring domains. If we look at Fig 1.2 we can see the difference between a material with uniform polarization and a material with domains. Neighbouring domains have polarization of opposite sign to limit the net surface charge. We can see how this is achieved by looking at Fig 1.2b. Along the surface we have an alternating direction of polarization, and an alternating negative bound charge and positive bound charge. The overall charge of the surface is zero.

What separates each domain is a domain wall (DW). Figure 1.2b shows a close up of a domain wall. We can see that the polarization of each domain is parallel to the DW. This is a neutral DW because there is as much negative charge as positive charge from the dipole moments accumulated at the DW.

Different Types of Domain Walls

While it is more favorable for a system to have polarization parallel to the DW, it is possible for different configurations to exist. Figure 1.3 and 1.4 shows possible configurations. Figure 1.3a shows the neutral 180-degree DW mentioned previously. Figure 1.3b shows a charged

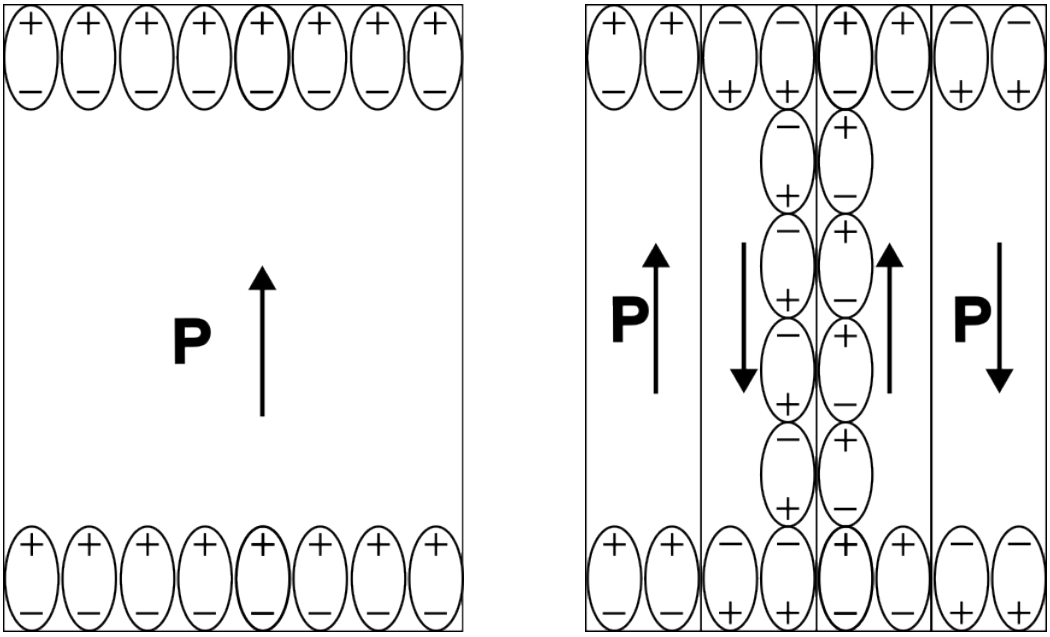

(a) (b)

Figure 1.2: (a) depicts a uniform domain with only the dipoles on the surfaces illustrated. (b) depicts neutral 180-degree domain walls with only the dipoles along the surface and inner domain wall illustrated. For both cases there are dipole moments throughout the whole material but these are not all illustrated

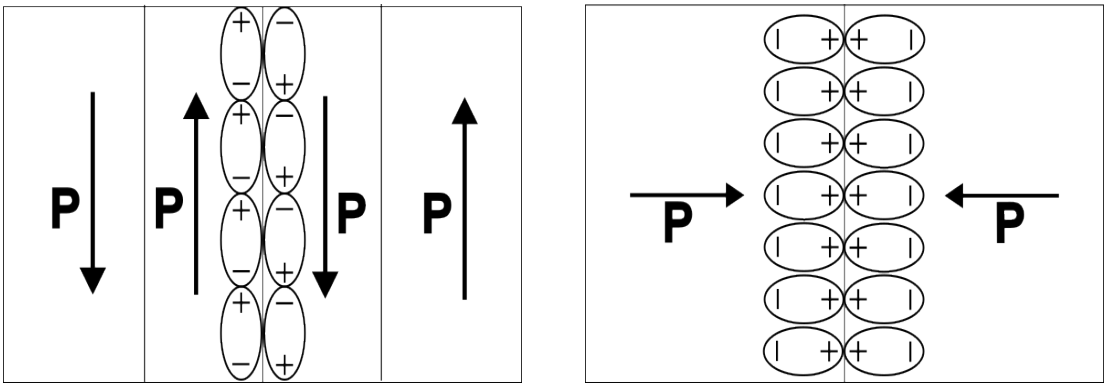

(a) (b)

Figure 1.3: (a) depicts a 180-degree neutral domain wall configuration. The polarization is parallel to the domain wall, thus the dipoles lie in an alternating configuration with an even distribution of negative and positive bound charge. (b) depicts a charged H-T-H domain wall configuration. The polarization is perpendicular to the domain wall, which results in the positive bound charge lining up at the domain wall.

180-degree head-to-head (H-T-H) DW. Figure 1.4a shows a neutral 90-degree head-to-tail (H-T-T) DW. Figure 1.4b shows a charged 90-degree H-T-H DW and a charged 90-degree tail-to-tail (T-T-T) DW. In Fig 1.4b, the DWs where the polarization vectors meet are the

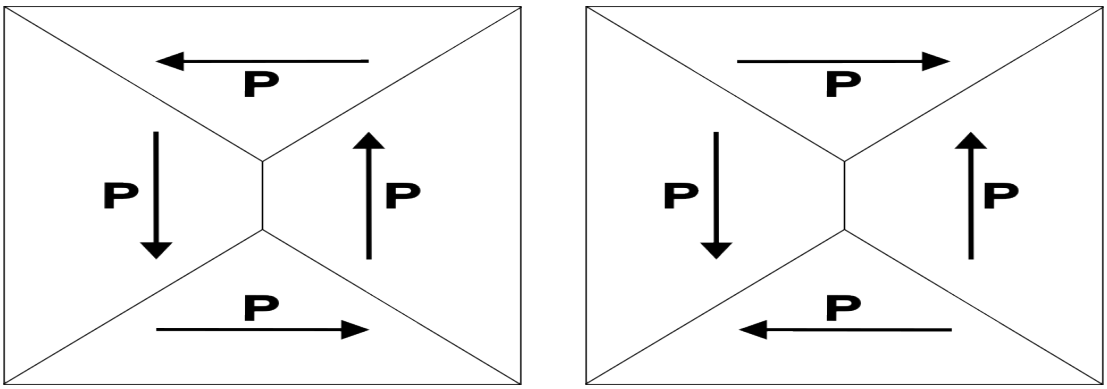

(a) (b)

Figure 1.4: (a) depicts 90-degree neutral domain wall configurations. This has vanishing charge at the domain walls and surfaces. (b) depicts 90-degree charged domain walls. There is a vanishing charge at the surface but the domain walls are positively charged (for H-T-H) and negatively charged (for T-T-T).

H-T-H DWs and the DWs where the polarization vectors point away from are the T-T-T DWs.

Charged Domain Walls

The idea of charged domain walls (CDWs) has been around since the 1970s, and with experimental imaging techniques such as transmission electron microscopy (TEM) charged domains walls were observed in the 1980s [10,11]. With advances in experimental techniques of imaging and manufacturing in the 21st century, the study of CDWs has gained a lot of interest [7, 8]. High resolution scanning TEM allows individual atomic displacement to be seen [12]. This means one can see the cations shift within unit cells, and can, therefore, see the polarization changing.

In a H-T-H configuration, as illustrated by Fig 1.3b and Fig 1.4b there is a component of the polarization that is normal to the domain wall. With the polarization facing towards the domain wall, the DW now carries an abundance of positive bound charge, making it a charged DW. In Fig 1.3b the abundance of positive bound charge comes from the positive ends of the dipole moments lined up at the DW. These produce an electric field which destabilizes the DW. However, if we introduce free electrons (or free charge) into the system we can stabilize the H-T-H configuration. The free electrons will accumulate at the

charged DW to screen the positive charge and stabilize the configuration. Electrons, holes, and mobile ions can all screen charge. In this thesis we add a free electron gas to our system by hand and focus on positively charged domain walls (H-T-H configuration).

The definition of the bound charge density, ρ_b, is

$$\rho_b = -\nabla \cdot P, \tag{1.2}$$

which is why there is bound charge at the DW, since there is a change in the polarization. The positive bound charge at the DW will generate an electric field acting in the opposite direction of the polarization, reducing the polarization. This electric field is referred to as a depolarizing field. However, if the bound charge is sufficiently screened by the free electrons then the depolarizing field is negligible and the polarization is unchanged. The accumulation of free charge along the DW leads to a highly conductive channel with the dimensions of the DW (2D sheet). It has been shown experimentally that the conductivity is $10^5 - 10^{13}$ times greater in a H-T-H configuration when compared to at T-T-T configuration [13, 14], because the T-T-T DW is negatively charged there is no accumulation of free electrons.

Materials such as $PbTiO_3$ can exhibit a CDW but have a T-T-T configuration in addition to H-T-H [15–17]. This system is in contrast to a H-T-H configuration and relies on oxygen vacancies as the source of screening. While still considered a CDW it does not have the same level of conductivity as a charged DW with a H-T-H configuration.

Response to Bias Voltage

A key feature of ferroelectric materials is their response to an external electric field. By applying an electric field to a ferroeletric material we can change the magnitude and directions of its polarization. When the electric field is turned off, the polarization persists.

Electric fields can also be used to manipulate CDWs. This has been shown experimentally and is the mechanism behind the idea of writable electronics [8]. One can apply an external electric field and move the CDW, which is conductive, essentially creating a movable nano-wire that can be used in circuitry.

1.2.3 Experimental Work

Here, we review some experimental work looking into the properties and applications of CDWs. For a more exhaustive list of applications refer to review article [18].

While CDWs have attractive properties and could be used to make new technology, the process for generating them needs to be predictable and reproducible. Right now CDWs are not easy to make and there is still more to learn about how they form. Huang *et al.* proposed a reliable way to produce a CDW by applying mechanical stress in ultra-thin $BaTiO_3$ [19]. The configuration they were able to reliably produce is what they refer to as a head/tail-to-body. While it is not the configuration we have been talking about it, it is still classified as a CDW.

One of the reasons for the sudden interest in CDWs is that detailed information about the CDWs can then be obtained from imaging techniques with nanoscale resolution. This imaging technique allows one to see individual atoms and their position relative to each other. Jia *et al.* used high resolution TEM to view the crystal unit cells in $Pb(Zr,Ti)O_3$ thin films [12], and measure the cation-oxygen dipole moments. A H-T-H CDW configuration was observed. Denneulin *et al.* used TEM to investigate $BaTiO_3$ thin-film growth on a substrate [20]. They were able to image ferroelectric domains, but more importantly showed that the boundary conditions in a TEM lamella can alter the domain structure.

As mentioned earlier, the reason for the large interest in CDWs is their high conductivity compared to other other DW configurations. Sluka *et al.* measured the conductivity of different DW configurations in the ferroelectric $BaTiO_3$ [13]. They took conductivity measurements through the bulk of the material, along a T-T-T CDW, and along a H-T-H CDW. As expected, the conductivity through the bulk of the material was negligible and almost identical to the conductivity of the T-T-T CDW. Since a T-T-T CDW is constructed from the negative ends of the polarization dipole moment, this would repel any free electrons but attract any oxygen vacancies which aren't conducting. The conductivity for the H-T-H CDW was measured to be 10^5 times greater than the others. $BaTi0_3$ is the material that we will focus on in this thesis. Werner *et al.* measured the conductivity of $LiNbO_3$ with a H-T-H CDW [14]. With a conservative estimate they found the conductivity of the H-T-H

CDW to be 10^{13} greater than the bulk material.

The main motivation for CDW research is due to its application for re-configurable conducting channels in nano-devices, in other terms writable electronics. Experiments have shown that it is possible to configure a material such that an external electric field can create a CDW from what was a previously neutral system [8]. When the electric field is turned off the material is left in a highly conductive state, which is stable. The conduction can be tuned by an applied voltage, which will increase or decrease the length of the CDW. The conductive state can be erased by applying a voltage in the opposite direction. Risch *et al.* have also created highly conductive rewritable channels (in a CDW) in $Pb(Zr,Ti)O_3$ with metallic-like properties [21]. McConville *et al.* have created a DW enabled memristor in thin-film $LiNbO_3$ [22].

1.2.4 Theoretical Work

Here, we review previous theoretical work. For a more exhaustive survey refer to the review article [23].

Luk'yanchuk *et al* looked into the formation of DWs and why the neutral 180-degree configuration is favourable [24]. Referring back to Fig. 1.2, we know that the configuration in Fig. 1.2a would be ideal in terms of ferroelectric performance. However, this configuration leads to a large depolarizing field that is comparable to the polarization but acts in the opposite direction. Figure 1.2b is energetically favourable because it minimizes the net surface charge, by alternating the polarization and thus alternating the local surface charge. Luk'yanchuk *et al.* showed theoretically that the depolarizing field for this case is confined to the surface. This significantly lowers the electrostatic energy of the system.

Gureev *et al.* looked at the energy required for a system to form charged domain walls [25]. A uniform or monodomain polarization (as referred to in the paper) is not energetically favorable and without screening charge (free electrons for example) the system will form neutral 180-degree domain walls (multidomain state). This can be seen in Fig. 1.2b. Gureev *et al.* found that the H-T-H or T-T-T (charged domain) configuration can be energetically favourable if the polarization is sufficiently large to generate screening charge from hole excitation. If the charged domain state is not favourable, the system will still

want to form neutral 180-degree domains.

Later work done by Gureev *et al.* looked at the force on a charged domain wall due to an external electric field [26]. They arrived at a general equation for the force that depends on the electric field, polarization, and free charge density,

$$p = \Delta F(P) + E(\sigma_f - \Delta P), \tag{1.3}$$

where p is the pressure, $\Delta F(P)$ is the difference in free energy of P between the two domains, ΔP is the difference in polarization, E_i is the electric field, σ_f is the free charge density. It is unclear how far a CDW would move based on the pressure from an external electric field. However, this equation does indicate what direction the CDW is expected to move. In this thesis we show that a positively charged DW will move against the direction of the external electric field, which is consistent with the findings of Chapman *et al.* [27].

1.2.5 Objectives

Theoretical work can answer questions about the mechanics of charged domain walls. In order to properly represent the physics, a theoretical model is needed. One motivation for this thesis is to find an efficient way to calculate the properties of a CDW. Sturman *et al.* proposed two approximations that simplify the calculations considerably [4]. With these approximations, they would calculate the properties analytically in certain limits. Without these approximations the properties must be obtained numerically, which takes considerable time. So, one of the questions we aim to answer in this thesis is, are these approximations good? Do they give us the same results when compared to the exact numerical solutions?

There is a 'universal' picture of a CDW in theoretical work [4, 25]. This universal CDW is often depicted as residing in an infinite thickness film, charge neutral, and with no bias voltage applied. However, in experiment CDWs are shown with none of these assumptions. CDWs are produced in thin or ultra-thin films, the CDW is not charge neutral, and a bias voltage is being applied as it is the main mechanism for their desired property. We look to calculate the properties of CDWs of physical interest. What happens when we vary the sample size? What happens when the CDW is not charge neutral? What happens when

we apply a bias voltage? How does this compare to experiment?

Chapter 2

Theory

2.1 Model

We are interested in a ferroelectric material with a head-to-head (H-T-H) polarization configuration and with free electrons. CDWs can be created with various geometries, we have chosen a simple geometry to model how a CDW moves under bias voltage. The ferroelectric material (blue) has two capacitor plates (grey) on either end connected to an external voltage. This is illustrated in Fig 2.1.

We only consider the z-component of the polarization. From experiments $BaTiO_3$ was shown to have a 90 degree H-T-H DW as well as a 90 degree T-T-T DW [13]. We focus on the H-T-H DW as it is conducting. While $BaTiO_3$ polarization has a y-component and z-component, there is no change in the y-component along y or z. In the Landau-Ginsburg-Devonshire (LGD) equation all contributions from the y-component would be constant, so we are still able to model the system without including it. Similarly, in Gauss's law we do not need to consider the y-component of the polarization since the electric field only has a z-component.

Since we only consider the z-component of polarization, the polarization vector is defined as $\mathbf{P} = P(z)\hat{k}$. The system has a finite length L in the z-direction and translational invariance in the x-direction and y-direction. This means that we can represent the system as a 1-D problem in LGD theory. We impose the boundary conditions

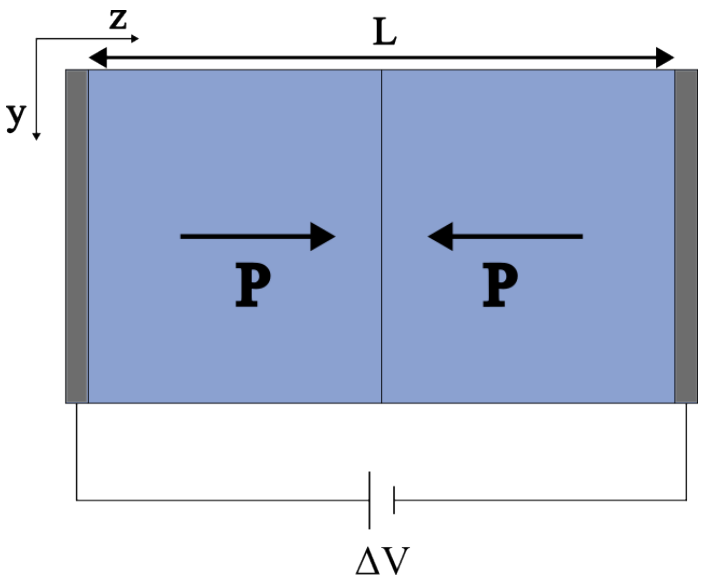

Figure 2.1: Illustration of the CDW model. A ferroelectric material (blue) between two capacitor plates (grey) which are connected to an external voltage source. The system has a length L. Polarization points along the z-axis. The DW is shown as a line separating the two domains with opposite polarization.

$$\frac{dP}{dz}|_{z=0} = \frac{dP}{dz}|_{z=L} = 0 \tag{2.1}$$

for simplicity in our calculations since we are only concerned with what is happening at the DW.

There is an external voltage source, ΔV, which is kept at zero for the initial set of results. When we look at the effect of a bias voltage in the second part of the results, ΔV will vary. We define the bias voltage as the change in voltage across the system, from left to right. We impose the boundary conditions

$$\phi(0) = V, \quad \phi(L) = 0. \tag{2.2}$$

The free electrons added to the system have a two-dimensional electron density, n_{2d}. We define n_{2d} as

$$n_{2d} = \int_0^L n(z)dz \tag{2.3}$$

where $n(z)$ is the three-dimensional electron density. The electrons are modelled using a

discrete Schrodinger's equation. Since the electric potential depends only on the z, we use separation of variables to re-write Schrodinger's equation to depend on z. We impose the boundary condition that the electron wave functions must vanish at $z = 0$ and $z = L$, and therefore the 2D electron density must vanish at $z = 0$ and $z = L$.

2.2 Landau-Ginzburg-Devonshire Theory

To describe the polarization, we turn to Landau-Ginzburg-Devonshire (LGD) theory. This theory describes the phase transition of a system near a critical point or temperature. More specifically this theory describes the free energy of the system in terms of an order parameter. In this case the order parameter is the polarization, where above the critical temperature the polarization is zero and below the critical temperature the polarization is non-zero. The critical temperature (T_c) is specific to each material. For example T_c is approximately 608 K for Pb(Zr,Ti)O_3. Below 608 K Pb(Zr,Ti)O_3 has a spontaneous polarization and each unit cell has a dipole moment, and above 608 K there is no spontaneous polarization.

We can find a solution for the spontaneous polarization by minimizing the free energy equation. The equation for the free energy is an expansion in powers of the order parameter, with coefficients that can be fitted to experiments. Equation 2.4 shows a simplified free energy for a system with uniform polarization and no electric field. The simplified free energy is

$$F_P = (a_1 P^2 + a_{11} P^4 + a_{111} P^6) \cdot V \tag{2.4}$$

where a_1, a_{11}, a_{111} are material-specific coefficients, V is the volume, and P is the polarization (order parameter). There are only even powers of the order parameter since the direction of the polarization does not affect the free energy in the absense of an electric field.

If all the coefficients are positive, the system is in a paraelectric phase with $P = 0$ at the minimum free energy. The a_{111} coefficient must be positive so there is a lower bound to the free energy, if not the series continues to a higher order. To get a non-zero solution to the polarization, a phase transition into the ferroelectric phase must occur, which is

achieved by lowering the temperature. There are two types of phase transitions. The first is continuous and the second is discontinuous. The continuous phase transition occurs when the a_1 coefficient becomes negative as the temperature is lowered while a_{11} is positive. The a_1 coefficient can be written as $a_1 = a_0(T - T_c)$. As the temperature is reduced from above the critical temperature, the coefficient goes from positive, to zero, then to negative. When a_1 is negative, there exists a minimum in the free energy for a non-zero solution to the polarization. The discontinuous phase transition is described by an abrupt appearance of non-zero polarization as the temperature is lowered.

Fig 2.2 illustrates how the free energy equation evolves as the temperature changes for each type of phase transition.

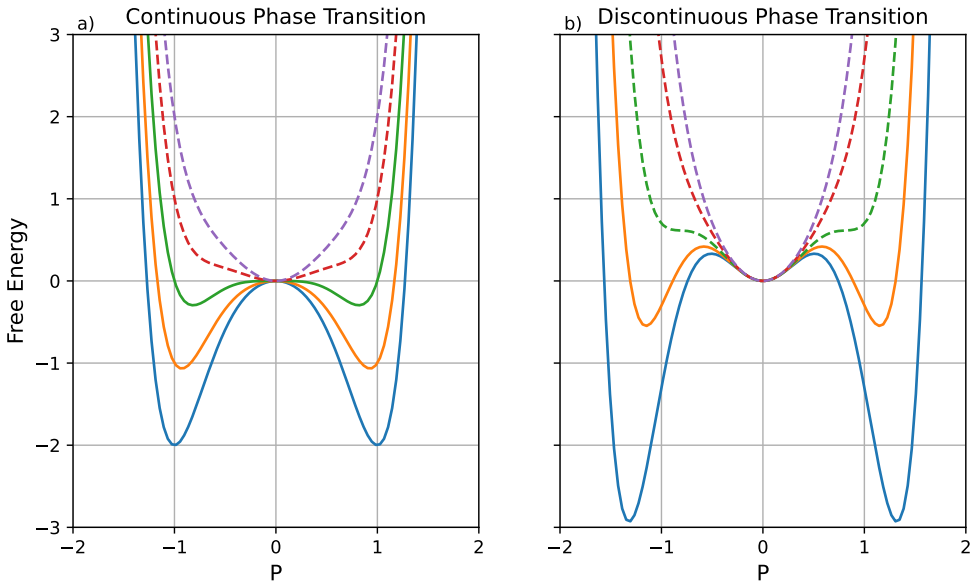

Figure 2.2: Dotted lines show the free energy for $T > T_c$. Solid lines show the free energy for $T < T_c$. The line color represents the free energy at different temperatures, in descending order, where the purple line is the highest temperature and the blue line is the lowest temperature. (a) shows how the free energy progresses for a continuous phase transition for arbitrary P. (b) shows how the free energy progresses for a discontinuous phase transition for arbitrary P.

Figure 2.2a shows the free energy progression for a continuous phase transition. One can see that at $T > T_c$ there is a minimum free energy at $P = 0$. When $T < T_c$ we then have a minimum when P is non-zero. Figure 2.2b shows the free energy progression for a discontinuous phase transition. When $T > T_c$ there is a minimum free energy at $P = 0$.

At $T = T_c$ there are three local minima, with two solutions for non-zero polarization as well as the previous $P = 0$ solution. As soon as $T < T_c$ the two local minima for non-zero polarization become lower in energy and are energetically favorable.

Equation 2.4 describes a system with uniform polarization. In practice ferroelectrics do not have uniform polarization, but instead have domains with alternating polarization. We need to account for domains by adding another term to the free energy. The term was introduced by Landau and Ginzburg and is $\frac{1}{2}\sum_{ijkl}\gamma_{ijkl}\frac{\partial P_i}{\partial z_j}\frac{\partial P_k}{\partial z_l}$. Since we are only concerned with a one dimensional problem this can be simplified and the free energy is

$$F_P = \int [a_1 P^2 + a_{11} P^4 + a_{111} P^6 + \gamma(\frac{dP}{dz})^2] d^3 r \tag{2.5}$$

where γ is another material-specific coefficient.

The coefficient γ is related to the correlation length, ξ, of the material. The larger the derivative of P the larger the free energy. When $T < T_c$ the correlation length is a length scale over which polarization varies. The equation for the correlation length is

$$\xi = \sqrt{\frac{\gamma}{2|a_1|}} \tag{2.6}$$

and it determines the width of neutral domain walls. This equation holds when $a_{111} = 0$.

To see the role of the correlation length we can solve for the polarization analytically. First we take the variational derivative of the free energy with respect to the polarization. To minimize the free energy we set the variational derivative equal to zero. Note the 6th order term has been dropped since $a_{11} > 0$ and $a_1 < 0$, and because $a_{11} > 0$ this term limits the equation as it guarantees a lower bound for the free energy.

$$\delta F = \int dr^3 \left[2a_1 P + 4a_{11} P^3 - 2\gamma \frac{d^2 P}{dz^2} \right] \delta P = 0 \tag{2.7}$$

For this equation to be satisfied for an arbitrary δP, everything in the brackets needs to be equal to 0.

$$\frac{\delta F}{\delta P} = 2a_1 P + 4a_{11} P^3 - 2\gamma \frac{d^2 P}{dz^2} = 0 \tag{2.8}$$

We can show that a solution to Eq.2.8 takes on the form of

$$P(z) = P_0 \tanh(\frac{z}{\xi}) \tag{2.9}$$

where P_0 is the bulk polarization and ξ is the correlation length.

The double derivative of P is

$$\frac{d^2P(z)}{dz^2} = P_0 \frac{-2}{\xi^2} \tanh(\frac{z}{\xi}) \operatorname{sech}^2(\frac{z}{\xi}) \tag{2.10}$$

which we insert into Eq.2.8 to get

$$P_0 \frac{4\gamma}{\xi^2} \tanh(\frac{z}{\xi}) \operatorname{sech}^2(\frac{z}{\xi}) + 2a_1 P_0 \tanh(\frac{z}{\xi}) + 4a_{11} P_0^3 \tanh^3(\frac{z}{\xi}) = 0. \tag{2.11}$$

Simplifying and using the identity $\operatorname{sech}^2(x) = 1 - \tanh^2(x)$ leads to

$$\frac{+2\gamma}{\xi^2}(1 - \tanh^2(\frac{z}{\xi})) + a_1 + 2a_{11} P_0^2 \tanh^2(\frac{z}{\xi}) = 0 \tag{2.12}$$

and then to

$$\tanh^2(\frac{z}{\xi})(2a_{11}P_0^2 - \frac{2\gamma}{\xi^2}) + (\frac{2\gamma}{\xi^2} + a_1) = 0. \tag{2.13}$$

Equation 2.13 takes on the form $a \tanh^2 \frac{z}{\xi} + b = 0$ and for the equation to be true for any z then $a = b = 0$.

$$(2a_{11}P_0^2 - \frac{2\gamma}{\xi^2}) = (\frac{2\gamma}{\xi^2} + a_1) = 0 \tag{2.14}$$

We can then solve for ξ

$$\xi = \sqrt{\frac{\gamma}{2|a_1|}}. \tag{2.15}$$

This shows where Eq.2.6 comes from and allows us to also solve for P_0.

$$P_0 = \sqrt{\frac{|a_1|}{2a_{11}}} \tag{2.16}$$

The solution to Eq.2.8 is

$$P(z) = \sqrt{\frac{a_1}{2a_{11}}} \tanh(\frac{z}{\xi}). \tag{2.17}$$

Equation 2.17 describes the polarization in a system with neutral domain walls and no free electrons.

To describe the polarization in a system with charged domain walls and free electrons we need to account for the electric fields due to bound and free charge. Depolarizing fields are an important consideration when considering H-T-H DWs, the system we are interested in, as they destroy polarization. We explain next how we account for the depolarizing field coming from the bound charge, and the effect of free charge.

First we consider the equation for the electric displacement.

$$D = \epsilon_\infty E + P \longrightarrow E = \frac{1}{\epsilon_\infty}(D - P) \tag{2.18}$$

where E is the total electric field in the system. Usually one will see this equation with ϵ_0 rather than ϵ_∞, and this will be explained later. In Eq. 2.18, $-\frac{P}{\epsilon_\infty}$ is the depolarizing field and $\frac{D}{\epsilon_\infty}$ is the electric field coming from all charges except the bound charge. This means that $\frac{D}{\epsilon_\infty}$ accounts for the external field applied through the capacitor plates as well as the charge from the free electrons. The total electric field is coupled to the polarization in the free energy equation and is dependant on the sign of the polarization. The energy of an electric field is

$$U = \frac{\epsilon_\infty}{2} \int |E|^2 d^3r \tag{2.19}$$

in a material with a background dielectric constant ϵ_∞.

If we substitute in Eq.2.18, we get

$$U = \frac{1}{2\epsilon_\infty} \int [D^2 + P^2 - 2D \cdot P] d^3r \tag{2.20}$$

where the D^2 term can be dropped because it does not depend on P. We can then update the free energy equation to

$$F = A\int_0^L dz[a_1P^2 + a_{11}P^4 + a_{111}P^6 - \frac{DP}{\epsilon_\infty} + \frac{P^2}{2\epsilon_\infty} + \gamma(\frac{dP}{dz})^2]. \tag{2.21}$$

We can collect like terms to simplify it further so the final version of the free energy is

$$F = A\int_0^L dz\left[\left(a_1 + \frac{1}{2\epsilon_\infty}\right)P^2 + a_{11}P^4 + a_{111}P^6 - \frac{DP}{\epsilon_\infty} + \gamma\left(\frac{dP}{dz}\right)^2\right] \tag{2.22}$$

Now that we have the free energy equation with the relevant terms we solve for the polarization at the minimum free energy. We set the variational derivative equal to zero

$$\frac{\delta F}{\delta P} = 0 = (2a_1 + \frac{1}{\epsilon_\infty})P + 4a_{11}P^3 + 6a_{111}P^5 - \frac{D}{\epsilon_\infty} - 2\gamma(\frac{d^2P}{dz^2}) \tag{2.23}$$

We use a numerical Galerkin-Newton Gradient Algorithm (GNGA) method to solve for the polarization.

In this section we have outlined how the polarization is modelled with LGD theory in the calculations for this thesis. We use a simplified LGD free energy equation to model the complexity of a H-T-H polarization configuration. Even though we are only considering the z-component of the polarization to be a function of z, this is similar to what is seen in experiment [13].

2.2.1 Background Dielectric Constant

The quantity ϵ_∞ has an important meaning and requires some explanation. A ferroelectric material exhibits the property of having spontaneous polarization. The spontaneous polarization arises from the phonon mode responsible for displacement of the central cation and oxygen atoms of the crystal unit cell becoming soft, below a critical temperature. The spontaneous polarization can be referred to as the critical polarization, but there are other non-critical contributions to the polarization that arise from the presence of an electric field. In the presence of an electric field non-ferroelectric phonon modes will respond to the electric field and polarize the lattice. This is a much smaller contribution than the critical contribution to the polarization [28]. The non-critical contributions are referred to

as the background polarization and a simple term can be added to the electric displacement equation to account for them.

$$D = \epsilon_0 E + (P + P_b) \tag{2.24}$$

where P_b is the background polarization and $P_b = \epsilon_0 \chi E$, where χ is the dielectric susceptibility. Now we can replace P_b in Eq. 2.24 and collect like terms so that

$$D = \epsilon_0 E + \epsilon_0 \chi E + P = \epsilon_0 (1 + \chi) E + P. \tag{2.25}$$

We let $\epsilon_\infty = \epsilon_0(1 + \chi)$. We can now rewrite the electric displacement equation as

$$D = \epsilon_\infty E + P. \tag{2.26}$$

2.3 Fourier Space

We have chosen to work in Fourier space rather than real space. Working in Fourier space means that we represent our functions as series of trigonometric functions. We define the Fourier series for a function $f(z)$ as

$$f(z) = a_0 + \sum_{n=1}^{N} a_n \cos \frac{n\pi z}{L} + \sum_{n=1}^{N} b_n \sin \frac{n\pi z}{L} \tag{2.27}$$

Where a_0, a_n, and b_n are coefficients defined by

$$a_0 = \sqrt{\frac{1}{L}} \int_0^L f(z) dz \tag{2.28}$$

$$a_n = \sqrt{\frac{2}{L}} \int_0^L f(z) \cos \frac{n\pi z}{L} dz \tag{2.29}$$

$$b_n = \sqrt{\frac{2}{L}} \int_0^L f(z) \sin \frac{n\pi z}{L} dz. \tag{2.30}$$

To simplify terms moving forward we define two functions, $c_n(z)$ and $s_n(z)$ as

$$c_n(z) = \begin{cases} \frac{1}{\sqrt{L}} & n = 0 \\ \sqrt{\frac{2}{L}} \cos k_n z & n > 0 \end{cases} \tag{2.31}$$

and

$$s_n(z) = \sqrt{\frac{2}{L}} \sin k_n z \quad n \geq 1 \tag{2.32}$$

with $k_n = \frac{n\pi}{L}$. We can now write a_n and b_n as

$$a_n = \int_0^L c_n(z) f(z) dz \tag{2.33}$$

and

$$b_n = \int_0^L s_n(z) f(z) dz \tag{2.34}$$

With the boundary conditions

$$\frac{dP_z}{dz}(z = 0) = \frac{dP_z}{dz}(z = L) = 0 \tag{2.35}$$

we do not consider the sine term in the series, which leads to the polarization function

$$P(z) = \sum_{n=0}^{N} p_n c_n(z) \tag{2.36}$$

where p_n are the Fourier coefficients associated with the polarization series. To solve for the p_n coefficients given a $P(z)$ we can use the equation

$$p_n = \int_0^L P(z) c_n(z). \tag{2.37}$$

We can calculate the bound charge density, ρ_b, using p_n from Eq.2.37.

$$\rho_b(z) = -\frac{dP}{dz} = \sum_{n=0}^{N} p_n k_n s_n(z) \tag{2.38}$$

Since P is directly related to ρ_b we can use the same Fourier coefficients (p_n) to calculate

each quantity. If, for example, we want to calculate ρ_f (the free charge density), we use a new set of Fourier coefficients, q_n. We define ρ_f as

$$\rho_f(z) = \frac{dD}{dz} = \sum_{n=1}^{N} q_n s_n(z). \tag{2.39}$$

We can calculate q_n from

$$q_n = \int_0^L \rho_f(z) s_n(z). \tag{2.40}$$

With q_n and p_n we can calculate the electric displacement, electric field, and electric potential by computing their Fourier series, shown in Section 2.4.

Working in Fourier space avoids having to calculate discrete derivatives and allows one to calculate any quantity we want with q_n and p_n.

2.4 Gauss's Law

To solve for the electric potential and electric field of the system we use Gauss's law,

$$-\epsilon_\infty \frac{d^2\phi}{dz^2} = \rho_f(z) + \rho_b(z). \tag{2.41}$$

ρ_f is the free charge density, ρ_b is the bound charge density, ϕ is the electric potential, and $\epsilon_\infty = 1 + \chi$ (see Eq.2.25) . We impose the boundary conditions

$$\phi(0) = \Delta V,\ \phi(L) = 0. \tag{2.42}$$

The bound charge density and polarization have the relation

$$\frac{-dP}{dz} = \rho_b \tag{2.43}$$

which allows one to write ρ_b as the Fourier series

$$\rho_b = -\frac{dP}{dz} = \sum_{n=1}^{N} p_n k_n s_n(z). \tag{2.44}$$

The free electron density comes from solving Schrodinger's equation for the electron

wave functions. This implies the same boundary conditions, that the free electron density must vanish at $z = 0$ and $z = L$. This allows one to write ρ_f as

$$\rho_f = \frac{dD}{dz} = \sum_{n=1}^{N} q_n s_n(z), \tag{2.45}$$

only taking on the sine component of the Fourier series because of the boundary conditions. We can solve for D by integrating Eq.2.45

$$\int dD = \int \sum_{n=1}^{N} [q_n s_n(z)]\, dz \tag{2.46}$$

which we can then solve for D as

$$D(z) = B - \sum_{n=1}^{N} \left[\frac{q_n}{k_n} c_n(z) \right] \tag{2.47}$$

Where B is an integration constant, obtained below.

From Gauss's law we can solve for the electric field and electric potential by integration. First we substitute Eq.2.44 and Eq.2.45 into Eq.2.41.

$$-\epsilon_\infty \frac{d^2\phi}{dz^2} = \sum_{n=1}^{N} (q_n + p_n k_n) s_n(z) \tag{2.48}$$

After integrating twice we get an equation for the electric potential

$$\phi(z) = a + bz + \frac{1}{\epsilon_\infty} \sum_{n=1}^{N} \frac{(q_n + p_n k_n)}{k_n^2} s_n(z). \tag{2.49}$$

We can then apply the boundary conditions to get

$$\phi(z) = V[1 - \frac{z}{L}] + \frac{1}{\epsilon_\infty} \sum_{n=1}^{N} \frac{(q_n + p_n k_n)}{k_n^2} s_n(z). \tag{2.50}$$

To get an equation for the electric field we can take the derivative of Eq. 2.50 with respect to z

$$E(z) = \frac{-d\phi(z)}{dz} = \frac{V}{L} - \frac{1}{\epsilon_\infty} \sum_{n=1}^{N} \frac{(q_n + p_n k_n)}{k_n} \sqrt{\frac{2}{L}} \cos(k_n z). \tag{2.51}$$

Then, the displacement is

$$\frac{1}{\epsilon_\infty}D(z) = \frac{V}{L} - \frac{1}{\epsilon_\infty}\sum_{n=1}^{N}\frac{q_n}{k_n}c_n(z) \tag{2.52}$$

and

$$\frac{1}{\epsilon_\infty}P(z) = \frac{1}{\epsilon_\infty}\sum_{n=1}^{N}p_n c_n(z). \tag{2.53}$$

2.5 Galerkin Newton Gradient Algorithm

We use a Galerkin Newton Gradient Algorithm (GNGA), which is an iterative method to numerically solve for the polarization in the LGD equation. Given an approximate solution, p_n^{old} (the Fourier coefficients described in Section 2.3), the algorithm will give an updated solution, p_n^{new}. A Newton algorithm is a numerical root finding method. We are trying to find a polarization that minimizes the free energy. To do this we find the root of the derivative of the free energy equation. A Galerkin method converts a continuous operator problem into a discrete problem with finite sets of basis functions. In this case we are taking a continuous polarization function and converting it to a set of basis functions in the form of a Fourier series. For a further description of the GNGA method refer to the paper by Neuberger *et al.* [29]. We will discuss how it is applied in our calculations here.

First, we start with our LGD free energy equation

$$F = A\int_0^L \left[\frac{\gamma}{2}\left(\frac{dP}{dz}\right)^2 + \left(a_1 + \frac{1}{2\epsilon_\infty}\right)P^2 + a_{11}P^4 + a_{111}P^6 - \frac{DP}{\epsilon_\infty}\right]dz \tag{2.54}$$

where

$$P(z) = \sum_{n=0}^{N}p_n c_n(z). \tag{2.55}$$

The idea is that starting from the functional one can take a partial derivative

$$g_j(p) = \frac{dF}{dp_j} \tag{2.56}$$

such that there exists a solution to P that minimizes the free energy when $g_j(p) = 0$ for all

j, where p is the set of Fourier components, $\{p_1, p_2, ..., p_n\}$, for the Fourier series of P. If we know g_j at some point p_0, we can estimate g_j at some nearby point p using a Taylor series.

$$g_j(p) = g_j(p_0) + \sum_k (p - p_0)_k \frac{\partial g_j}{\partial p_k} \tag{2.57}$$

If p_0 is a guess for the solution $g_j(p) = 0$ then Eq. 2.57 allows us to find an improved estimate for the root of $g_j(p)$ by setting $g_j(p) = 0$. We define $\frac{\partial g_j}{\partial p_k} = A_{jk}$ to rewrite Eq. 2.57 as

$$g_j(p_0) + \sum_k (p - p_0)_k A_{jk} = 0. \tag{2.58}$$

We can write this as a matrix equation and rearrange for p to get

$$p = p_0 - A^{-1} g \tag{2.59}$$

which essentially says that we can calculate a new p with a given p_0 (which is a guess for p), where A and g are calculated using p_0. Then p becomes p_0 and the process is repeated until one finds a p where $g_j(p) = 0$. As $g_j(p)$ approaches 0, p_0 approaches p and we arrive at a solution. The problem with this is that one can overshoot the solution if p_0 is not close to the answer. To fix this problem, a mixing parameter δ is introduced which multiplies the $A^{-1}g$ term.

$$p = p_0 - \delta A^{-1} g \tag{2.60}$$

The goal of δ is to make the change to p with each iteration smaller, so the solution is not skipped over.

This algorithm is used solely to solve for the polarization at fixed electron density. The iterative method for obtaining self-consistency between the polarization and electron density is outlined in Section 3.1. Here we will explain the GNGA and then explain how to calculate g and A.

1. Calculate g and A
2. Calculate $A^{-1}g$.

3. Update p. $p = p_0 - \delta A^{-1} g$. We set $\delta = 0.05$. Different values for δ were tested, but this value seemed to be the best for arriving at a solution in a timely manner.

4. Update P with p by computing the Fourier series, Eq. 2.55.

5. Update loop counter

6. Check for convergence by calculating the mean of $|A^{-1}g|/|p_n|$. The convergence criteria is met when the ratio of the mean of $|A^{-1}g|/|p_n|$ becomes smaller than a number set by hand. We chose a ratio of 10^{-4} to determine convergence. The smaller the number the longer the run time, but if it is not strict enough then the solution will never properly converge. We tested a range of values from 10^{-2} - 10^{-8} and settled on 10^{-4} as it provided a converged solution in the shortest amount of time.

7. If convergence is met then p and P will be updated in the main algorithm. If convergence is not met then using the updated p and P we return to step 1 and calculate a new g and A.

Now we calculate g and A starting from Eq. 2.54.

$$\begin{aligned} g_j(P) = \frac{dF}{dp_j} = \int_0^L \Big[& -\gamma \frac{dP}{dz} k_j s_j(z) + (2a_1 + \frac{1}{\epsilon_\infty}) P(z) c_j(z) \\ & + 4a_{11} P(z)^3 c_j(z) + 6a_{111} P(z)^5 c_j(z) - \frac{D}{\epsilon_\infty} c_j(z) \Big] dz \end{aligned} \tag{2.61}$$

where

$$\frac{d}{dp_j}(\frac{dP}{dz})^2 = 2\frac{dP}{dz}\frac{\frac{dP}{dz}}{dp_j} = -2\frac{dP}{dz} k_j s_j(z) \tag{2.62}$$

and

$$\frac{d}{dp_j} P^2 = 2P\frac{dP}{dp_j} = 2P c_j(z) \tag{2.63}$$

and then the same can be applied for the quartic and sextic terms. We can then simplify this starting with

$$\frac{dP}{dz} = -\sum_{n=1}^{N} p_n k_n s_n(z) \tag{2.64}$$

and

$$D = \frac{V}{L} - \sum_{n=1}^{N} \frac{q_n}{k_n} c_n(z). \tag{2.65}$$

Since the sum in D starts at $n = 1$, because of k_n in the denominator, we need to make a special case for g and A for $n = 0$ and $n \neq 0$. The $c_n(z)$ and $s_n(z)$ functions account for each case, but when calculating g and A, each case needs to be explicitly calculated. If we put Eq. 2.64 and Eq. 2.65 back into Eq. 2.61 we get

$$\begin{aligned} g_j(P) = \frac{dF}{dp_j} = \int_0^L \Bigg[\gamma \sum_{n=0}^{N} p_n k_n k_j s_n(z) s_j(z) \\ +(2a_1 + \frac{1}{\epsilon_\infty}) \sum_{n=0}^{N} p_j c_n(z) c_j(z) + 4a_{11} P(z)^3 c_j(z) \\ +6a_{111} P(z)^5 c_j(z) + \sum_{n=1}^{N} \frac{q_n}{k_n \epsilon_\infty} c_n(z) c_j(z) \Bigg] dz \end{aligned} \tag{2.66}$$

We then evaluate the integral in Eq.2.61. The first term only has a non-zero answer when $n = j$. Then we consider $\int_0^L \cos(k_n z) \cos(k_j z) = \frac{L}{2} \delta_{n,j}$, which simplifies a few terms. We leave the cubic and quintic terms in integral form. The final equation for $g_j(P)$ when $j = 0$ is

$$g_0(P) = \frac{\partial F}{\partial p_0} = [2a_1]\, p_0 + \int_0^L \left[4a_{11} P(z)^3 c_0(z) + 6a_{111} P(z)^5 c_0(z) \right] dz. \tag{2.67}$$

and for $j \neq 0$

$$\begin{aligned} g_j(P) = \frac{\partial F}{\partial p_j} = \left[\gamma k_j^2 + 2a_1 + \frac{1}{\epsilon_\infty} \right] p_j + \frac{q_j}{k_j \epsilon_\infty} \\ + \int_0^L [4a_{11} P(z)^3 c_j(z) + 6a_{111} P(z)^5 c_j(z)] dz. \end{aligned} \tag{2.68}$$

Now we calculate A, which will take on a matrix form. To simplify the calculation we only take the diagonal of the A matrix, as we are still able to achieve convergence. If we considered every matrix element we might reach convergence in fewer steps, but the

computation time would be far greater. We can express A_{jj} for $j = 0$ as

$$A_{00}(P) = \frac{d^2F}{dp_0 dp_0} = [2a_1] + \int_0^L \left[12a_{11}P(z)^2 c_0^2(z) + 30a_{111}P(z)^4 c_0^2(z)\right] dz. \tag{2.69}$$

and for $j \neq 0$ as

$$\begin{aligned} A_{jj}(P) = \frac{d^2F}{dp_j dp_j} = \left[\gamma k_j^2 + 2a_1 + \frac{1}{\epsilon_\infty}\right] \\ + \int_0^L \left[12a_{11}P(z)^2 c_j^2(z) + 30a_{111}P(z)^4 c_j^2(z)\right] dz. \end{aligned} \tag{2.70}$$

Now that we have g_j and A_{jj} we can implement the algorithm.

2.6 Discrete Schrodinger's Equation

To model the free electrons in the system we use Schrodinger's equation

$$-\frac{\hbar^2}{2m^*}(\partial_x^2 + \partial_y^2 + \partial_z^2)\Psi(x,y,z) - e\phi(z)\Psi(x,y,z) = \epsilon\Psi(x,y,z) \tag{2.71}$$

where Ψ is the wave function, ϕ is the potential, e is the electric charge, and ϵ is the eigenvalue.

Since ϕ only depends on z, we can use separation of variables to rewrite the wave function as

$$\Psi(x,y,z) = \frac{1}{\sqrt{A}} e^{i(k_x x + k_y y)} Z^{(n)}(z). \tag{2.72}$$

We can also write the energy for a band n as

$$\epsilon_{n,k_x,k_y} = \tilde{\epsilon_n} + \frac{\hbar^2}{2m^*}(k_x^2 + k_y^2) \tag{2.73}$$

with a wavevector (k_x, k_y), and where $\tilde{\epsilon_n}$ is the eigenvalue for the equation

$$-\frac{\hbar^2}{2m^*}\frac{d^2}{dz^2}Z^{(n)}(z) - e\phi(z)Z^{(n)}(z) = \tilde{\epsilon_n}Z^{(n)}(z) \tag{2.74}$$

where $Z^{(n)}$ is the n^{th} wave function. We also impose the hard-wall boundary conditions of

$$Z^{(n)}(0) = Z^{(n)}(L) = 0 \tag{2.75}$$

such that the wave function vanishes at the boundaries.

To solve Eq.2.74 we discretize the problem and solve the equation on a grid. The grid contains N points with index $i \in [0, N-1]$. The grid points are spaced by Δz, so the ith grid point is at $z_i = i\Delta z$ where

$$\Delta z = \frac{L}{N-1}. \tag{2.76}$$

The discrete approximation for the 2nd derivative is

$$\frac{d^2}{dz^2} Z^{(n)}(z_i) = \frac{Z^{(n)}_{i-1} + Z^{(n)}_{i+1} - 2Z^{(n)}_i}{(\Delta z)^2}. \tag{2.77}$$

There are problems calculating the end points of the grid since when $i = N$ we can not calculate $Z^{(n)}_{i+1}$ because it is out of bounds, similarly for $i = 0$ and $Z^{(n)}_{i-1}$. However, due to the boundary conditions we just need to solve the interior points of Z. This leads to solving Eq.2.74 as a $(N-2) \times (N-2)$ eigenvalue problem

$$\begin{bmatrix} a_1 & b & & & \\ b & a_2 & b & & \\ & b & a_3 & b & \\ & & & \dots & \\ & & & b & a_{N-2} \end{bmatrix} \begin{bmatrix} Z^{(n)}_1 \\ Z^{(n)}_2 \\ Z^{(n)}_3 \\ \dots \\ Z^{(n)}_{N-2} \end{bmatrix} = \tilde{\epsilon_n} \begin{bmatrix} Z^{(n)}_1 \\ Z^{(n)}_2 \\ Z^{(n)}_3 \\ \dots \\ Z^{(n)}_{N-2} \end{bmatrix}$$

where

$$a_j = \frac{\hbar^2}{m^*(\Delta z)^2} - e\phi(z_j) \tag{2.78}$$

$$b = -\frac{\hbar^2}{2m^*(\Delta z)^2} \tag{2.79}$$

Using a Python function from the Scipy library, *scipy.linalg.eigh_tridiagonal*(), we can

compute the eigenvalues and their corresponding eigenvectors from the matrix.

Chapter 3

Computational Method

In this chapter we outline the computational method for calculating the properties of a H-T-H CDW. We use an iterative process which numerically solves three main equations. The polarization is obtained from the LGD free energy equation, the electrons are modelled by Schrodinger's equation, and the electric field and electric potential are obtained from Gauss's Law.

3.1 Method

Step 1.

We set initial conditions and make initial guesses for P, ϕ, E, ρ_b, ρ_f, p_n, and q_n. These guesses are educated guesses as the performance of the algorithm highly depends on them.

$\boldsymbol{P}$: We use the solution for the polarization of an insulating ferroelectric as an initial guess, which is

$$P = -P_{bulk} \tanh(\frac{z - L/2}{\xi}) \tag{3.1}$$

where P_{bulk} is maximum polarization for the bulk of a specific material.

$\boldsymbol{\rho_f}$: We take the initial guess for the free charge density to be

$$\rho_f = \frac{-en_{2d}}{\cosh^2(\frac{z-L/2}{\xi})} \tag{3.2}$$

where e is the charge of an electron, n_{2d} is the two-dimensional electron density, L is the length of our system, and ξ is the correlation length. This comes from taking the derivative of P with respect to z to get $-\rho_b$, which we make the assumption is pretty close to ρ_f. The derivative of tanh gives us the general shape, and then P_{bulk} has the units of $[C/m^2]$, the same as en_{2d}.

$\boldsymbol{\phi}$: We take the initial guess for the electric potential to be

$$\phi = \frac{-1}{\cosh(\frac{z-L/2}{\xi})}. \tag{3.3}$$

After we set these initial guesses we can calculate the initial p_n, q_n, and $E(z)$. To get p_{n_i} and q_{n_i} we use Eq. 2.37. To get $E_i(z)$ we use $-\frac{d\phi_i}{dz} = E_i$.

Step 2.

We start the iterative process by solving Schrodinger's equation for the electron's eigenvalues and eigenvectors. This is done by solving a tridiagonal matrix, outlined in Section 2.6.

Step 3.

The next step in the iterative process is to calculate the chemical potential, μ, from summing over the Fermi-Dirac equation

$$n_{2d} = \frac{2}{A}\sum_{k_x,k_y,n} f(\epsilon_n, k_x, k_y) \tag{3.4}$$

$$n_{2d} = \frac{m^* k_b T}{\pi\hbar^2}\sum_{n} \ln\left[1 + e^{-\beta(\tilde{\epsilon_n}-\mu)}\right] \tag{3.5}$$

using a bisection method. Where n_{2d} is the two-dimensional electron density which we set by hand, β is $\frac{1}{k_b T}$, and $\tilde{\epsilon_n}$ are the eigenvalues.

Step 4.

We can now calculate ρ_f from

$$\rho_f(\mathbf{r}) = -en(\mathbf{r}) = -\frac{2e}{A\Delta z}\sum_{k_x,k_y,n} |\psi_{k_x,k_y,n}(\mathbf{r})|^2 f(\epsilon_n, k_x, k_y) \tag{3.6}$$

which simplifies to

$$\rho_f(z) = \frac{-em^* k_b T}{\Delta z \pi \hbar^2} \sum_n |Z_i^{(n)}|^2 \ln\left[1 + e^{-\beta(\tilde{\epsilon_n} - \mu)}\right] \tag{3.7}$$

using the chemical potential from Step 3, and the eigenvalues and eigenvectors for the electrons from Step 2. Z are the eigenvectors; the subscript i refers to each z location (grid point) and we sum over n eigenvectors for each z location.

With a new ρ_f calculated now we can calculate a new set of q_n values using the Fourier transform, Eq. 2.37.

Step 5.

Using the GNGA we are able to calculate the polarization P and a new set of p_n values.

Step 6.

Now with most of the quantities calculated we can update p_n and q_n, which is done by an Anderson Mixing method [30]. Once the p_n and q_n values are updated we can calculate a new $E(z)$ and $\phi(z)$ by simply calculating the Fourier series for each quantity. This marks the end of one iteration. The updated p_n, q_n, and ϕ are then used to start a new iteration. One thing to note is that the summation over n needs to be truncated. It turns out that high frequency Fourier coefficients are negligible in this scenario allowing n to be truncated at around $n = 200$, the value used for the calculations.

We arrive at a solution when convergence is achieved. Convergence is achieved when the difference in the new updated values and the old values approach zero. We define convergence as when the mean of $|P_{new} - P_{old}| = 10^{-6}$ and the mean of $|\phi_{new} - \phi_{old}| = 10^{-6}$.

3.2 Sturman Approximations

With the foundation laid out on how we can model a CDW, we take a look at the approximations Sturman *et al.* make [4].

3.2.1 Gradient Term Approximation

The first approximation is that the gradient term in the LGD equation can be discarded. This is shown in Eq. 3.8.

$$F_P = a_1 P^2 + a_{11} P^4 - EP + \gamma(\frac{dP}{dz})^2 \longrightarrow F_P = a_1 P^2 + a_{11} P^4 - EP \tag{3.8}$$

The reason they can discard this term is that due to the electron screening, the polarization does not change fast enough, or the derivative is not large enough, for this term to be significant [4, 25].

3.2.2 Gauss's Law Approximation

The second approximation is that the electric field term, $\epsilon_\infty E$, in Gauss's law can be dropped due to the smallness of the term [4]. This is shown in Eq. 3.9

$$D = \epsilon_\infty E + P \longrightarrow D = P \tag{3.9}$$

This is because $\epsilon_\infty << \frac{1}{a_1}$, which means that the background polarization coming from $\epsilon_\infty E$ is much less than the lattice polarization coming from P. The consequence of this approximation is that the bound charge density and free charge density are equal and opposite which is illustrated when we consider the other form of Gauss's Law

$$-\epsilon_\infty \frac{d^2\phi}{dz^2} = \rho_f(z) + \rho_b(z) \longrightarrow -\rho_f(z) = \rho_b(z). \tag{3.10}$$

This also implies that there is no electric field in the system. However, they use a simplified version of Landau theory

$$2a_1 P + 4a_{11} P^3 = E = -\frac{d\phi}{dz}, \tag{3.11}$$

to calculate the residual electric field and electric potential (based on the first approximation), in order to solve Schrodinger's equation. Their calculations are therefore not self-consistent. In our method we calculate the electric field directly from Gauss's Law which allows us to apply a bias voltage. Sturman's equations are not set up to add a bias voltage, and is not immediately obvious how that could be done.

3.2.3 Approximated Method

We will now go over the method for calculating CDW properties with these approximations in place. What must be noted is that Sturman *et al.* have semi-analytical equations to calculate properties such as polarization, electric potential, etc. When we present the results in Chapter 3, we do not use the equations in Sturman's paper, but rather apply their approximations to our method.

The approximations have a big effect on how properties of a CDW are calculated. The second approximation has the biggest effect on the run-time of the calculation, which improves 10-fold. The approximation allows us to scrap the GNGA method (the most time consuming part of the calculation) altogether because now we can relate free charge density and bound charge density. Since we are working in Fourier space this allows us to directly relate the Fourier coefficients p_n and q_n to each other. This will be shown in the following steps for the approximated method.

Step 1.

We start with the same initial guesses of P, ϕ, and ρ_f as our method in Section 2.7. Then using a Fourier transform, Eq.2.37, we can solve for an initial p_n and q_n. An initial electric field is calculated using the approximated LGD equation

$$E = a_1 P + a_{11} P^3. \tag{3.12}$$

Step 2.

We start the iterative process by calculating Schrodinger's equation for the electron's eigenvalues and eigenvectors, as before in Section 2.6.

Step 3.

The next step in the iterative process is to calculate the chemical potential, μ, as before.

Step 4.

We can now calculate ρ_f from

$$\rho_f(z) = \frac{-em^* k_b T}{\Delta z \pi \hbar^2} \sum_n |Z_i^{(n)}|^2 \ln\left[1 + e^{-\beta(\tilde{\epsilon_n} - \mu)}\right] \tag{3.13}$$

using the chemical potential from Step 3, and the eigenvalues and eigenvectors for the electrons from Step 2.

With a new ρ_f calculated now we can calculate a new set of q_n values using the Fourier transform, Eq. 2.37. Here is where the approximated method differs. We can calculate a new set of p_n values from the relation

$$p_n = \frac{q_n}{k_n} \tag{3.14}$$

and then a new P by computing the Fourier series for P with the new p_n.

Step 4.

We calculate a new electric field from

$$E = a_1 P + a_{11} P^3. \tag{3.15}$$

Since we do not have an electric field in Gauss's law we can not use p_n and q_n to calculate the electric field or electric potential. Instead we Fourier transform the electric field, using Eq. 2.37, to get a set of Fourier coefficients, e_n, for the electric field. Using the relation

$$\phi_n = \frac{e_n}{k_n} \tag{3.16}$$

we calculate the Fourier coefficients, ϕ_n, for the Fourier series to calculate a new electric potential

$$\phi(z) = \sum_{n=1}^{N} \phi_n s_n(z). \tag{3.17}$$

Step 5.

We check for convergence at the end of the iteration. Convergence is achieved when the difference in the new updated values and the old values approach zero. We define convergence as when the mean of $|P_{new} - P_{old}| = 10^{-6}$ and the mean of $|\phi_{new} - \phi_{old}| = 10^{-6}$. If convergence is not met then the updated ϕ is used to start a new iteration.

3.2.4 Key Parameters from Sturman's Paper

Apart from the approximations, there are some relevant parameters that Sturman *et al.* introduces in their paper. These ideas are discussed here.

As discussed in Section 3.2.1 and 3.2.2, the approximations made by Sturman *et al.* allow for the CDW properties, such as polarization, electric potential, electron density, etc, to be calculated analytically within certain limits. They find a single length scale, d

$$d = (2\hbar^2/m_e e|a_1|P_0)^{1/3} \tag{3.18}$$

which is specific to H-T-H CDWs. In Eq. 3.18, a_1 is a material specific coefficient in the LGD free energy equation, and P_0 is the saturated polarization, meaning $P(z)$ as z approaches ∞. Since a_1 and P_0 are both material specific, this means that each material will have its own d value. What this means is that d is now the relevant length scale for a H-T-H DW.

Sturman *et al.* also comes up with a parameter called Q which is used to classify the domain wall as quantum or quassi-classical. Q determines the number of localized levels in the wall, the binding energies of electrons, and the CDW width. They obtain

$$Q = \frac{4\pi P_0 d^2}{e}. \tag{3.19}$$

We will focus on the relation between Q and the DW width,

$$DW_{width} = 0.91 d Q^{2/5} \tag{3.20}$$

Equation 3.20 is Sturman's predicted DW width, but it is unclear what the criteria is for calculating the DW width. We define the calculated DW width as the length between $\pm 90\%$ of P_0. We will compare the predicted DW width with the calculated DW width from exact numerical solutions.

Chapter 4

Results

The results are split into two main sections. First, we look at the effects of the two approximations made by Sturman *et al.* We will compare results using Sturman's approximations with results from exact numerical solutions. Recall that Sturman's first approximation disregards the gradient term in the LGD free energy equation. The second approximation disregards the electric field term in Gauss's Law. Along with these approximations there are some assumptions that Sturman *et al.* makes. The assumptions are that the system has infinite length, no applied bias voltage, and as much bound charge as free charge. In the second section we compare results that go beyond Sturman's assumptions and approximations to results that fall under the limitations set by Sturman.

4.1 Approximations

For the first section of results we compare Sturman's approximations with exact numerical solutions. We start by solving all of the equations outlined in Chapter 2. We then incorporate Sturman's approximations one at a time to see the effect. This process is done for two theoretical materials, each with a different set of parameters. The parameters used come from Sturman's paper. The two sets of parameters are shown in Table 3.1. Real ferroelectric material parameters fall somewhere between the theoretical parameters used here.

P_0 [C/m^2]	a_1 [C^{-2}m^{2}N]	a_{11} [C^{-4}m^{6}N]	g_{11} [C^{-2}m^{4}N]	d [nm]	ξ [nm]	m^*
0.3	$-0.05 \times \frac{1}{4\pi\epsilon_\infty}$	$0.28 \times \frac{1}{4\pi\epsilon_\infty}$	4.17×10^{-10}	1.52	3.05	$0.2m_0$
0.02	-0.5 $\times \frac{1}{4\pi\epsilon_\infty}$	$625 \times \frac{1}{4\pi\epsilon_\infty}$	5.46×10^{-9}	1.74	3.49	$0.2m_0$

Table 4.1: Theoretical parameters. P_0 and a_1 taken from [4]. a_{11} comes from Eq.2.16. $\epsilon_\infty = (1+\chi)\epsilon_0 = 5 \cdot \epsilon_0$ [31]. $m_0 = 9.109 \times 10^{-31}$kg (mass of electron). d and ξ come from Eq.2.18 and Eq.2.6, respectively.

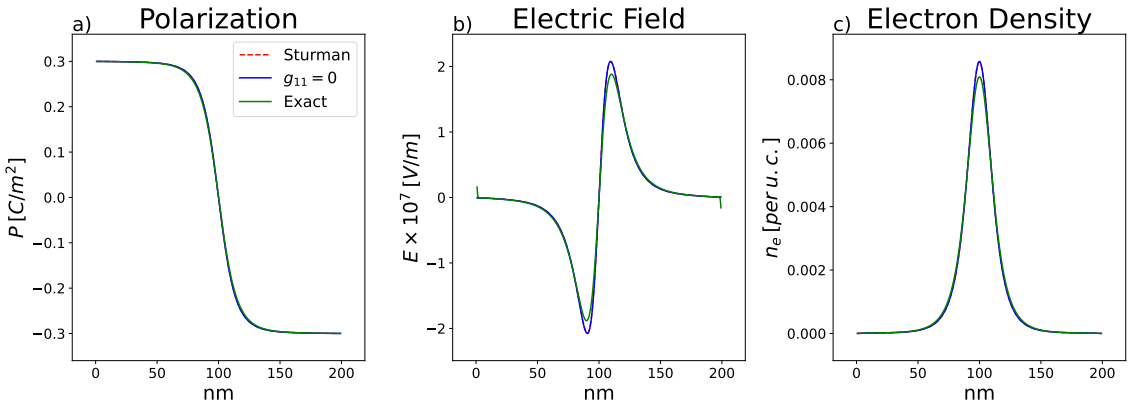

Figure 4.1: Comparison of the polarization, electric field, and electron density, using the first set of parameters in table 4.1. Curves labelled 'Sturman' show the profile using the approximations from Sturman *et al*, '$g_{11} = 0$' label shows the profile disregarding the gradient term, and curves labelled 'Exact' show the profile when no approximations are made.

Figure 4.1 shows the polarization, electric field, and electron density profiles as approximations are made to the exact solutions. The first thing to note is that a positive polarization indicates a direction pointing to the right and negative polarization indicates a direction pointing to the left. Figure 4.1 is therefore a H-T-H configuration. The polarization profile labelled 'Sturman' comes from using both of Sturman's approximations. The profile labelled '$g_{11} = 0$' comes from making the approximation that the gradient term in the LGD equation is zero. Finally, the profile labelled 'Exact' comes from the full numerical solution. The takeaway from this plot is that the first approximation disregarding the gradient term in the LGD equation, has a small effect. It changed the DW width which in turn has an effect on the electric field and electron density.

Figure 4.2 shows the same quantities as Fig. 4.1 but for different parameters, the second set in table 4.1. For this set of parameters we see a more significant difference due to the first approximation. This would suggest that the accuracy varies based on parameters (or

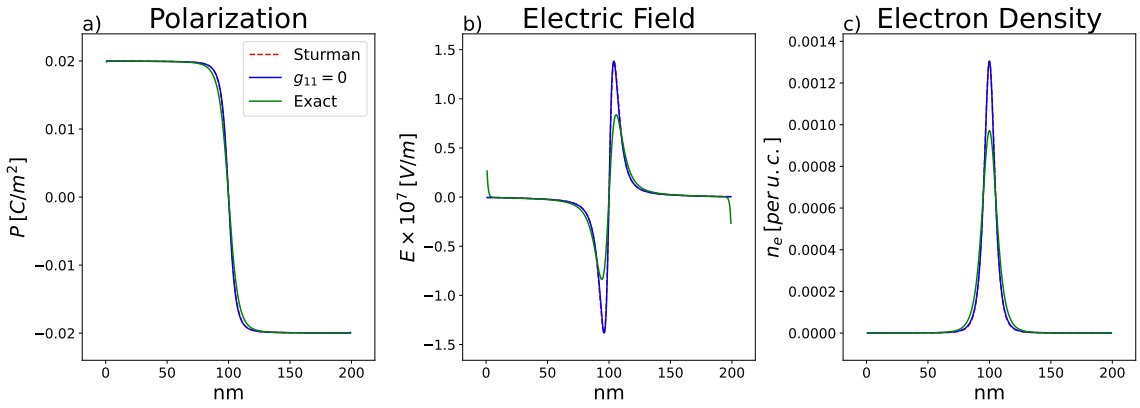

Figure 4.2: Comparison of the polarization, electric field, and electron density, using the second set of parameters in table 4.1. Curves labelled 'Sturman' show the profile using the approximations from Sturman *et al*, '$g_{11} = 0$' label shows the profile disregarding the gradient term, and curves labelled 'Exact' show the profile when no approximations are made.

material).

The approximations produce similar results to the exact solutions, for each set of parameters. The approximation of disregarding the gradient term in the LGD equation seems to have the biggest impact on the results. One could use these approximations to get fairly accurate solutions for a system within the scope of Sturman's limitations. In the next section we are going to go beyond the limitations of Sturman's assumptions to see how the results compare. The first assumption follows the approximation of dropping the electric field term in Gauss's law, it is assumed that there is as much bound charge as free charge. This is unlikely in actual practice, so we will look at solutions with varying n_{2d} values. The second assumption is that the system has infinite length, which is not realistic or practical for the applications of CDWs. Writable electronics is the main application for CDWs and there is already experimental data for systems on the order of 20nm [8]. We will look at the effects of shrinking the system size. Finally, the last assumption is that no bias voltage is applied. Again, with the application for CDW being writable electronics it is essential that a bias voltage is applied to move the DW. We will be applying a bias voltage to see how the DW responds.

4.2 Beyond Sturman's Assumptions

In this section we go beyond the assumptions made by Sturman to see how the results compare to those under the limitations set by Sturman. We start with the assumption that there is as much bound charge as free charge. To go beyond this assumption we will look at polarization, electric field, and electron density profiles for varying n_{2d} values. Starting with $n_{2d} = \frac{2P_{Bulk}}{e}$, to show the profiles for a system where the bound charge and free charge are equal, we will then lower the n_{2d} value to represent a more realistic system. Next we will look at the assumption that there is no bias voltage applied. To go beyond this limitation we will simply apply a bias voltage. We will also vary n_{2d} while applying a bias voltage. Real life systems will have different amounts of free charge so we want to see the effects of a bias voltage on systems with varying n_{2d} values. The final assumption is that the system has infinite length. However, experimental work on writable electronics looks at system sizes as small as 20nm. We will look at the effects of shrinking the system size, while also varying n_{2d} values and applying a bias voltage. This is the most realistic case of interest to experimental work.

We have also decided to use the parameters of a well known ferroelectric material, $BaTiO_3$, to try to represent a real material. This is a material that is heavily studied for its CDW. $BaTiO_3$ is a moderately polarized material with a $P_{Bulk} \approx 0.2 - 0.3[C/m^2]$ [32]. $BaTiO_3$ has a naturally occurring 90 degree H-T-H DW [13]. As explained in Chapter 2, we can still accurately model a 90 degree H-T-H DW since there is no change in polarization in the x direction which acts as a constant term in the LGD free energy equation.

n_{2d}

We are going to focus on one assumption in this subsection, that there is as much bound charge as free charge. In a real system there will most likely be less free charge than bound charge, so we will vary n_{2d}. Starting with $n_{2d} = 2\frac{P_{Bulk}}{e}$, namely a system where the bound charge and free charge are equal, we will then lower n_{2d} to represent a more realistic system. The other assumptions are not of concern in this subsection. To represent an infinite system we set $L = 200nm$. No bias voltage will be applied, so $\Delta V = 0$.

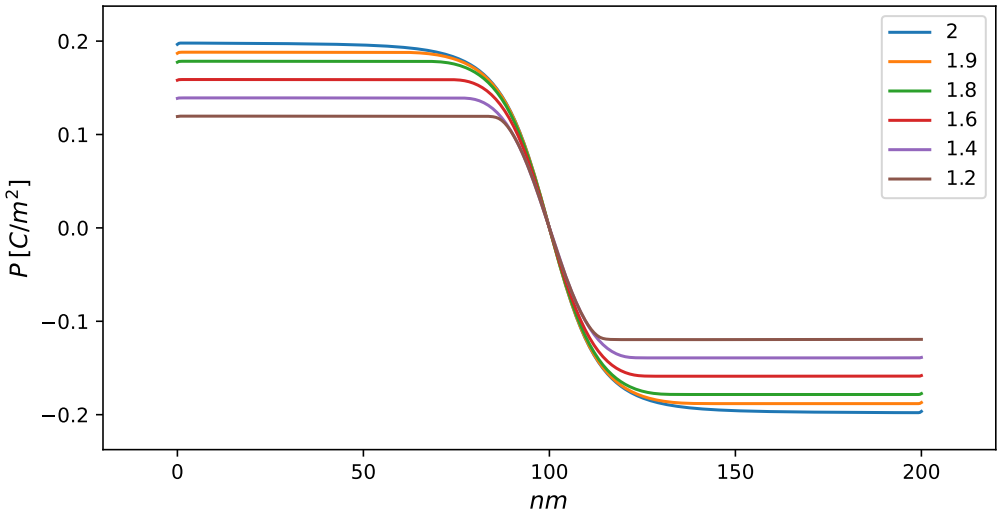

Figure 4.3: Polarization profiles for varying n_{2d} values at $\Delta V = 0V$. The numbers in the legend represent the factor of P_{Bulk} in the equation for n_{2d}, for example $n_{2d} = 2\frac{P_{Bulk}}{e}$.

Fig 4.3 shows different polarization profiles associated with different values of n_{2d}. The first profile labelled '2' would be considered the baseline, where there is as much bound charge as free charge. A n_{2d} value of $2\frac{P_{Bulk}}{e}$ is the electron density needed to screen the positive bound charge on the domain wall. Any n_{2d} value less than that would leave bound charge unscreened, leading to a depolarizing field that would reduce the polarization. This is evident in the rest of the profiles plotted, which are all for n_{2d} values less than $2\frac{P_{Bulk}}{e}$. As the value for n_{2d} is lowered we see a reduction in the polarization.

As n_{2d} is reduced, we see the profile of the polarization stray from the $\tanh \frac{z}{\xi} Q^{2/5}$ solution Sturman derives. This is most evident in the profile for $n_{2d} = 1.2\frac{P_{Bulk}}{e}$. We can also see the DW width get smaller as n_{2d} decreases.

Now we highlight how well Sturman's approximations do. Figure 4.4 shows polarization profiles for the exact solution and Sturman's approximation for the largest n_{2d} value, smallest n_{2d} value, and middle n_{2d} value. For a larger range of n_{2d} values, see the Appendix. One can see that for larger n_{2d} the results are nearly identical. For the smallest n_{2d} value there is a small but visible difference in the results, which is much more obvious in the electric field and electron density, shown below.

Figure 4.5 shows the electric field for each n_{2d} value at $\Delta V = 0$. Since there is no bias

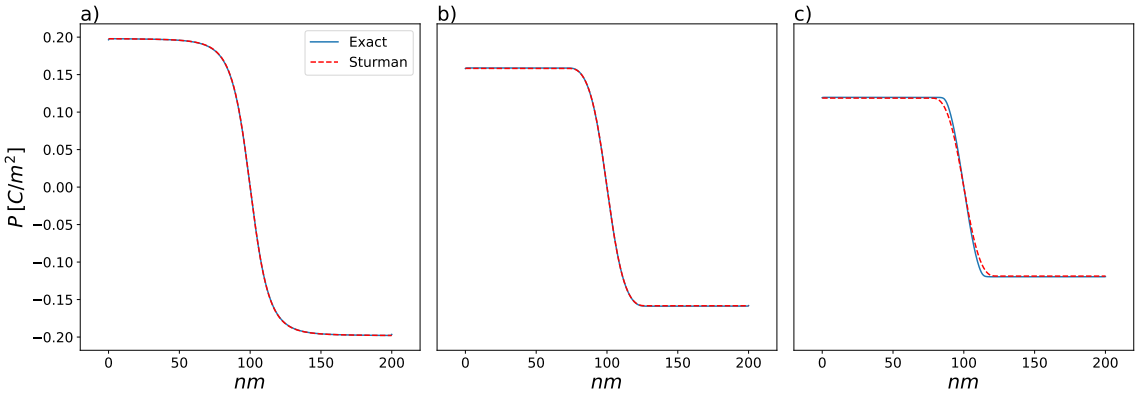

Figure 4.4: Polarization profile comparison for three n_{2d} values, $n_{2d} = 2\frac{P_{Bulk}}{e}$, $n_{2d} = 1.6\frac{P_{Bulk}}{e}$, $n_{2d} = 1.2\frac{P_{Bulk}}{e}$, from left to right. 'Our Method' is the polarization calculated using our complete method. 'Sturman' is the polarization calculated using both of the approximations found in [4].

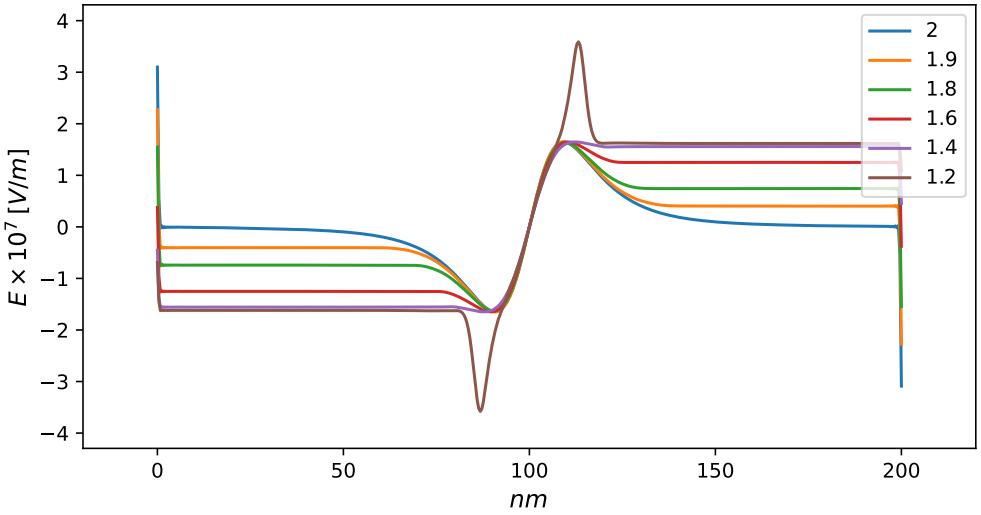

Figure 4.5: Electric field profiles for varying n_{2d} values at $\Delta V = 0V$. The numbers in the legend represent the factor of P_{Bulk} in the equation for n_{2d}, for example $n_{2d} = 2\frac{P_{Bulk}}{e}$.

voltage we see anti-symmetric electric field profiles. The electric field outside of the domain wall increases as n_{2d} is lowered. As the electron density decreases, the unscreened bound charge increases, producing a larger depolarizing field.

Similarly to Fig. 4.4, we look at how well Sturman's approximations do for the electric field at different n_{2d} values in Fig. 4.6. Again, we see nearly identical results for larger n_{2d} values. At small n_{2d} we can start to see a difference specifically in the DW region.

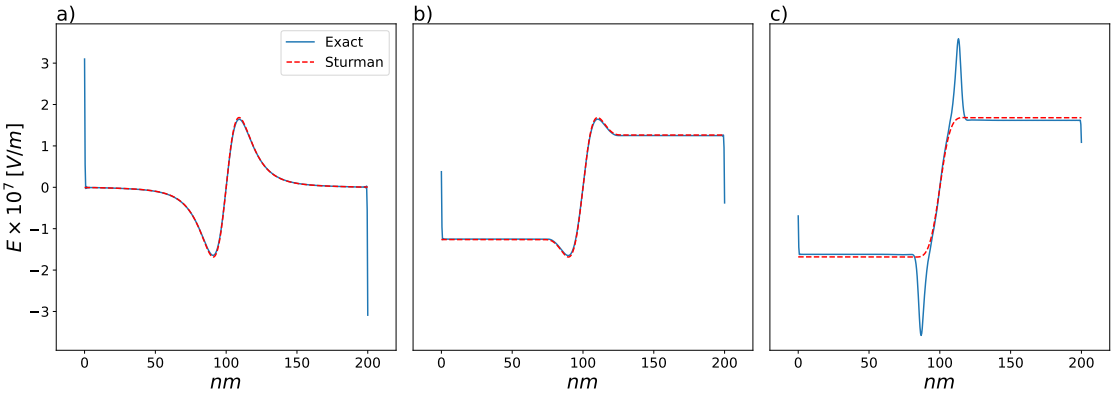

Figure 4.6: Electric field profile comparison for three n_{2d} values, $n_{2d} = 2\frac{P_{Bulk}}{e}$, $n_{2d} = 1.6\frac{P_{Bulk}}{e}$, $n_{2d} = 1.2\frac{P_{Bulk}}{e}$, from left to right. 'Our Method' is the electric field calculated using our complete method. 'Sturman' is the electric field calculated using both of the approximations found in [4].

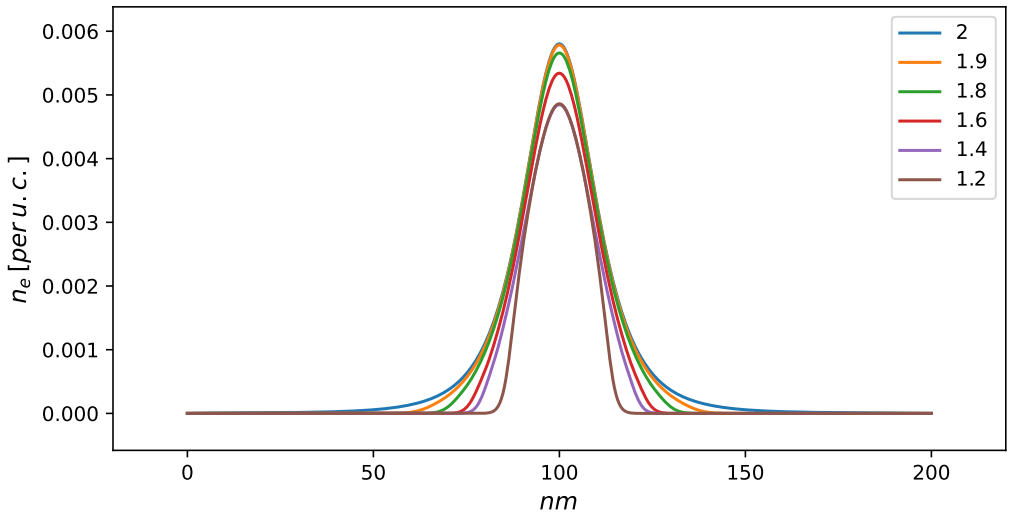

Figure 4.7: Electron density profiles for varying n_{2d} values at $\Delta V = 0V$. The numbers in the legend represent the factor of P_{Bulk} in the equation for n_{2d}, for example $n_{2d} = 2\frac{P_{Bulk}}{e}$.

Figure 4.7 shows the electron density profiles for varying n_{2d}. The main takeaway here is that as n_{2d} is lowered, the width of the electron distribution decreases. Even though the electron density is reduced by almost a half, the electron density peak does not change that much for each n_{2d} value, but instead the electrons become more concentrated at the DW.

Figure 4.8 compares Sturman's approximation to our exact solution. For larger n_{2d} values we see a negligible difference, but for the lowest n_{2d} value we can see a difference in

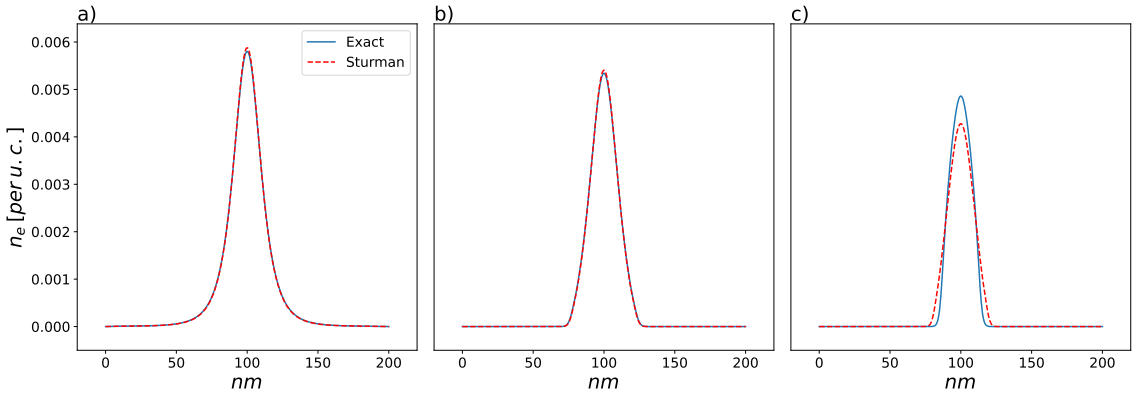

Figure 4.8: Electron density profile comparison for three n_{2d} values, $n_{2d} = 2\frac{P_{Bulk}}{e}$, $n_{2d} = 1.6\frac{P_{Bulk}}{e}$, $n_{2d} = 1.2\frac{P_{Bulk}}{e}$, from left to right. 'Our Method' is the electron density calculated using our complete method. 'Sturman' is the electron density calculated using both of the approximations found in [4].

the peak electron density and the distribution.

Overall the approximations made by Sturman do a pretty good job in capturing the physics of a CDW. For larger n_{2d} values we see almost no difference in the polarization, electric field, DW charge, and electron density. When we look at the lowest n_{2d} case we do see differences in the solutions. The assumption Sturman makes is that the bound charge and free charge are equal. When we go beyond this assumption and look at the case for the lowest n_{2d} value, we see the largest difference in the solutions. As a real material will most likely not have as much free charge as bound charge, the results suggest that this approximation and assumption would not be as reliable for real materials. The difference in the time it takes to run these calculations is also very significant. Depending on what one is trying to achieve, one could use Sturman's approximations and still get usable results.

Bias Voltage

Previously we looked at how well Sturman's approximations work for calculating the polarization, electric field, DW charge, and electron density for varying n_{2d}. The calculations were all done at $\Delta V = 0$ since Sturman's equations are not set up for a bias voltage. Now, we are going to see how a bias voltage affects these quantities at various n_{2d} values. This will be done exclusively with the exact numerical procedure from Sec 2.7. The aim for this

section is not to compare different methods but to go beyond Sturman's assumption and learn how a bias voltage affects the DW.

To help interpret our results we consider the equation

$$-\int_0^L E dz = \phi(L) - \phi(0). \tag{4.1}$$

Taking $\phi(L) = 0$ and $\phi(0) = V$, we can simplify to Eq. 4.1 to

$$\phi(0) = V = \int_0^L E dz. \tag{4.2}$$

The integral of the electric field must be equal to the bias voltage. We will see how the electric field changes from what is seen in Fig. 4.5 in order to satisfy Eq. 4.2 when a bias voltage is applied.

We will use Eq. 4.4 to calculate the charge on the DW to see how a bias voltage affects the charge. To get Eq. 4.4 we start with

$$\frac{dE}{dz} = \frac{\rho}{\epsilon_\infty} \longrightarrow \epsilon_\infty \int_0^L dE = \int_0^L \rho dz. \tag{4.3}$$

Which we can solve and get

$$(E(z = L) - E(z = 0))\epsilon_\infty = \sigma \tag{4.4}$$

where σ is the total charge (bound + free) with units $[C/m^2]$.

Similar to Fig 4.3, polarization profiles are plotted in Fig. 4.9 for various n_{2d}, except now $\Delta V = 1$V. Again, we see the reduction in the polarization due to the depolarizing field as n_{2d} is lowered. There is a bit more going on in this figure though.

The DW's of the first three profiles (labelled '2', '1.9', and '1.8') seem to sit on top of each other, but differ around $z = 0$. This uptick near $z = 0$ is due to electron spillover; the applied voltage pulls electrons off of the DW to the surface. The electrons are being pulled to surface rather than the DW, which is why we see the first three profiles sit on top of each other. This is more clearly seen in Fig 4.10. The reason why the electrons are pulled away from the DW is that they are not tightly bound. Fig 4.10 shows the electron density, and

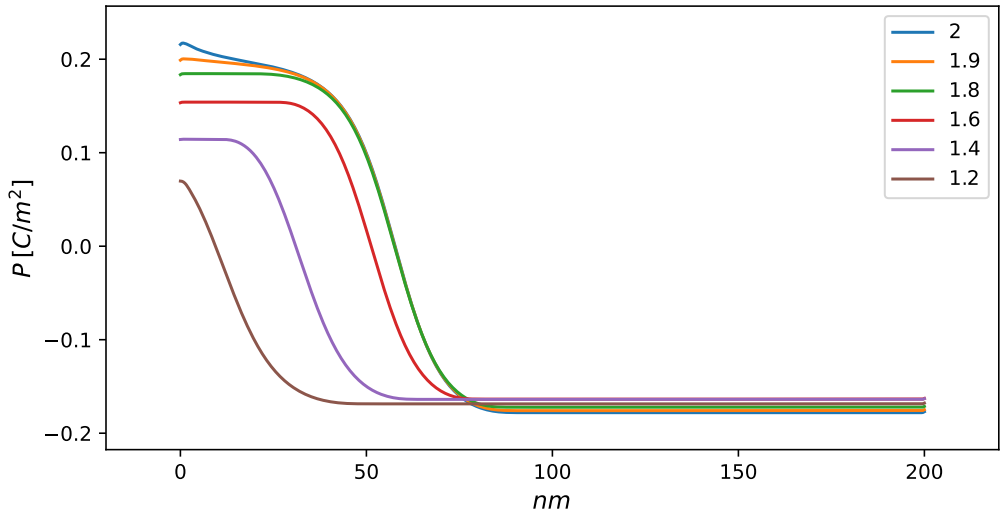

Figure 4.9: Polarization profiles for varying n_{2d} values at $\Delta V = 1V$. The numbers in the legend represent the factor of P_{Bulk} in the equation for n_{2d}, for example $n_{2d} = 2\frac{P_{Bulk}}{e}$.

the electron density for the first profile is much more spread out than the others. When $n_{2d} \leq 1.8\frac{P_{Bulk}}{e}$, the electrons become more concentrated at the DW and we do not see any spillover.

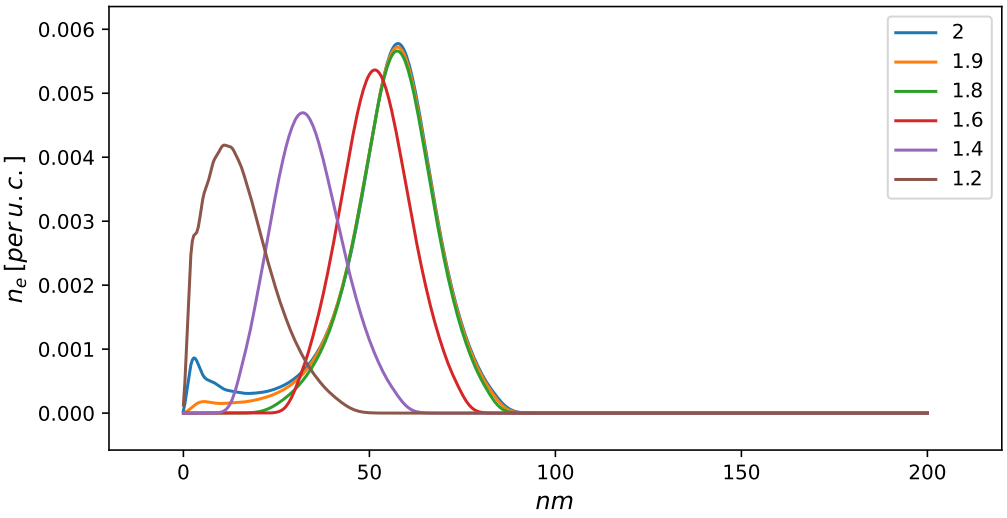

Figure 4.10: Electron density profiles for varying n_{2d} values at $\Delta V = 1V$. The numbers in the legend represent the factor of P_{Bulk} in the equation for n_{2d}, for example $n_{2d} = 2\frac{P_{Bulk}}{e}$.

Figure 4.10 shows the change in electron density as n_{2d} is lowered. While the electron density is reduced by almost half we see that the peak electron density does not change

significantly. In order for the peak to not significantly change, the distribution of the electrons becomes narrower.

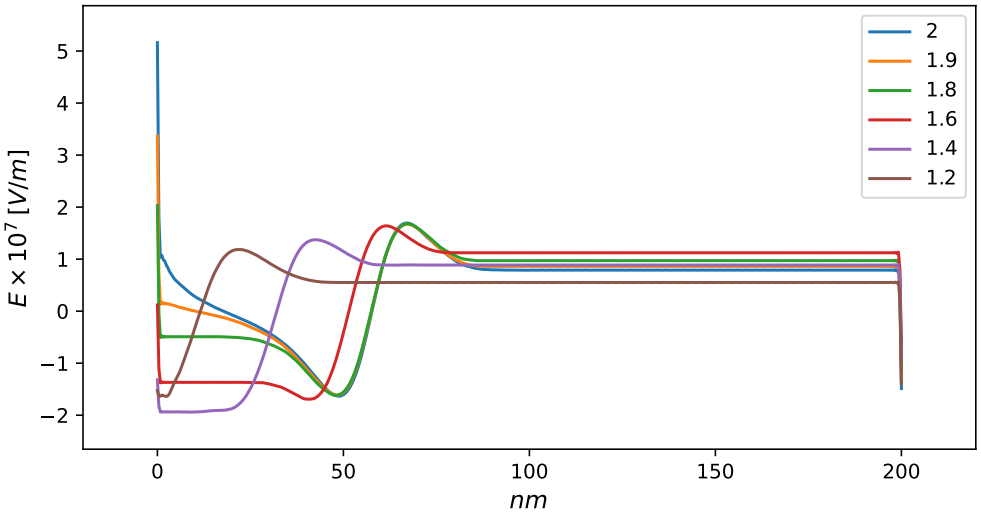

Figure 4.11: Electric field profiles for varying n_{2d} values at $\Delta V = 1V$. The numbers in the legend represent the factor of P_{Bulk} in the equation for n_{2d}, for example $n_{2d} = 2\frac{P_{Bulk}}{e}$.

σ_{DW}	$n_{2d} = 2.0\frac{P_{Bulk}}{e}$	1.9	1.8	1.6	1.4	1.2
$\Delta V = 0$	$0.01[\cdot 10^{-3}\, C/m^2]$	0.36	0.66	1.11	1.38	1.43
$\Delta V = 1$	$0.26[\cdot 10^{-3}\, C/m^2]$	0.39	0.65	1.1	1.25	0.97

Table 4.2: DW charge for varying n_{2d} values at $\Delta V = 0V$ and $1V$.

In Fig. 4.11 we see that once a bias voltage is applied the profiles are no longer anti-symmetrical. Equation 4.2 still must be satisfied and so the electric field can satisfy Eq. 4.2 in different ways. With a positive bias voltage, the positive region of the electric field profile needs to get larger and/or the negative region needs to get smaller. The first way this can happen is a shift in the DW to the left, which will shift the electric field profile to the left. The positive region will get bigger while the negative region gets smaller. The second way is for each point of the electric field profile to be greater, shifting the profile 'upwards'. A mixture of shifting horizontally and vertically is also possible. With a $\Delta V = 1$ the electric field satisfies Eq. 4.2 by primarily shifting horizontally, meaning the DW is shifted as well, and by shifting in the vertical direction.

Table 4.2 highlights the change in the DW charge when n_{2d} is changed and a bias voltage

is applied. For $\Delta V = 0V$ we see an overall increase in the charge on the domain wall as n_{2d} decreases. The charge on the DW becomes more positive with a bias voltage for the first two n_{2d} values. This correlates with the electrons being pulled from the DW to the surface, shown in Fig.4.10. The DW becomes less positive for the rest of the n_{2d} values when a bias voltage is applied. This is because the DW moves towards the surface and so the positive bound charge merges with the electrons that have been pulled to the surface.

So far we have talked about the effect of n_{2d} and bias voltage on the polarization, electric field, DW charge, and electron density each individually. However, these three quantities are all related and one quantity can not change without affecting the other. The question of "why does the DW moves the way it does when we apply a bias voltage?" is still un-answered.

n_{2d} Dependence

To summarize our results we have plotted some key quantities vs n_{2d} for $\Delta V = 0$ and $\Delta V = 1$.

In Fig. 4.12 we show DW charge, E_{right} (which is the maximum electric field outside of the DW region), DW width, and P_0 as a function of n_{2d} for $\Delta V = 0$. In panel a) we see the DW charge decrease as n_{2d} is increased, since we are adding more electrons to screen the positive bound charge. In panel b) we see the electric field decrease as n_{2d} is increased, due to the change in depolarizing fields from the un-screened bound charge. In panel c) we see the DW width increase as n_{2d} is increased. This is not consistent with Sturman's equation for DW width

$$DW_{width} = 0.9 \cdot d \cdot Q^{2/5} = 0.9 \cdot d \cdot \left(\frac{4\pi P_0 d^2}{e}\right)^{2/5}. \tag{4.5}$$

While his equation depends on P_0 in the numerator, d also depends on P_0 but decreases as P_0 increases. In panel d) we can see P_0 increase with n_{2d} which is expected as there is more screening of the bound charge, reducing the depolarizing effects.

Everything plotted in Fig. 4.13 is the same as Fig. 4.12 but for $\Delta V = 1$. The DW width and P_0 behave similarly as a function of n_{2d} as for the case of a zero bias voltage.

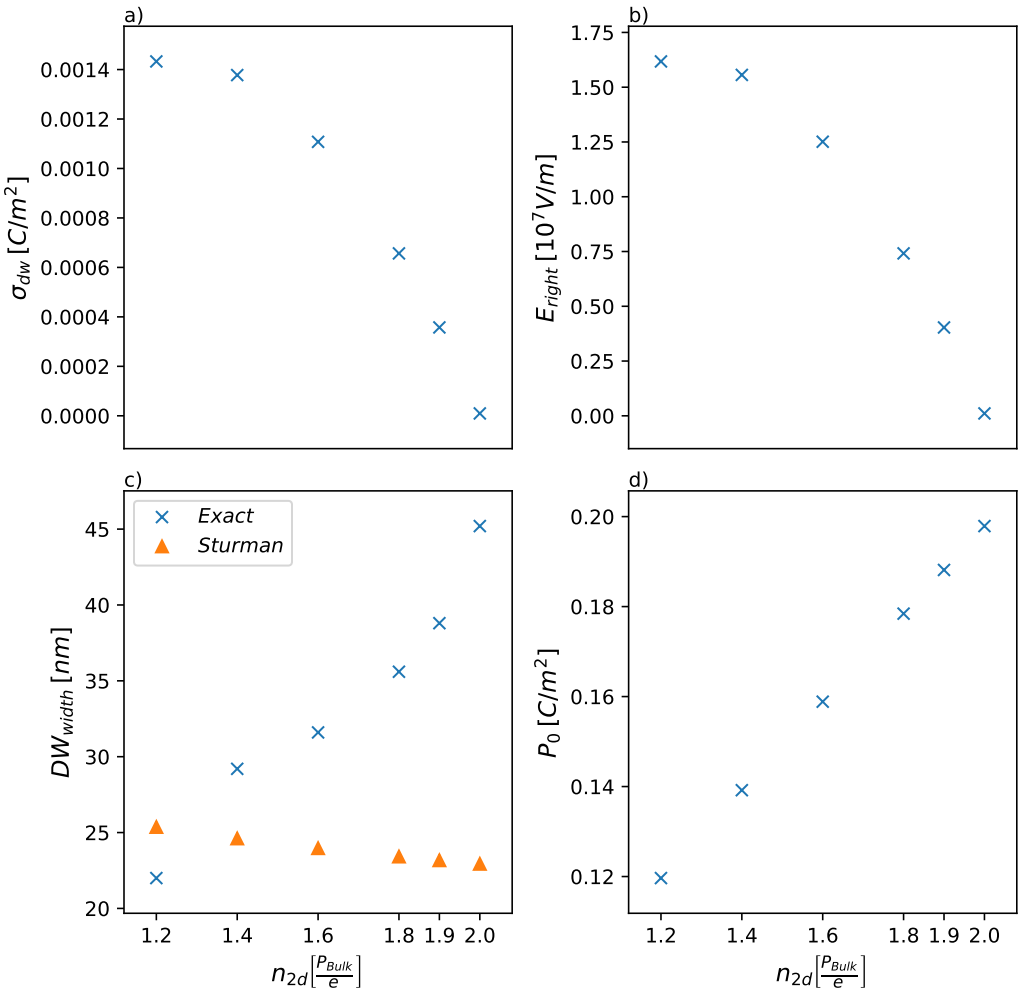

Figure 4.12: (a) σ_{DW} vs n_{2d}, where the points plotted are from Table 4.2. (b) E_{right} vs n_{2d}. The electric field away from the DW. (c) DW_{width} vs n_{2d}. 'Exact' is the DW width calculated by measuring z from 90% of P_{max} to 90% of P_{min}. 'Sturman' is the DW width from Eq. 4.5. (d) P_0 vs n_{2d}. All at $\Delta V = 0V$

The DW charge and electric field, on panel a) and b), behave differently though. The DW charge is seen to drop for $n_{2d} = 1.2\frac{P_{Bulk}}{e}$, and this was explained in the previous section. This is due to the DW shifting so far left that the electrons at the surface merge with the DW, effectively lowering the overall charge on the DW. The electric field increases with n_{2d} until $n_{2d} = 1.6\frac{P_{Bulk}}{e}$, and then decreases with n_{2d}. This is explained with Eq.4.2, the electric field is able to satisfy Eq.4.2 by shifting horizontally or vertically. For example the

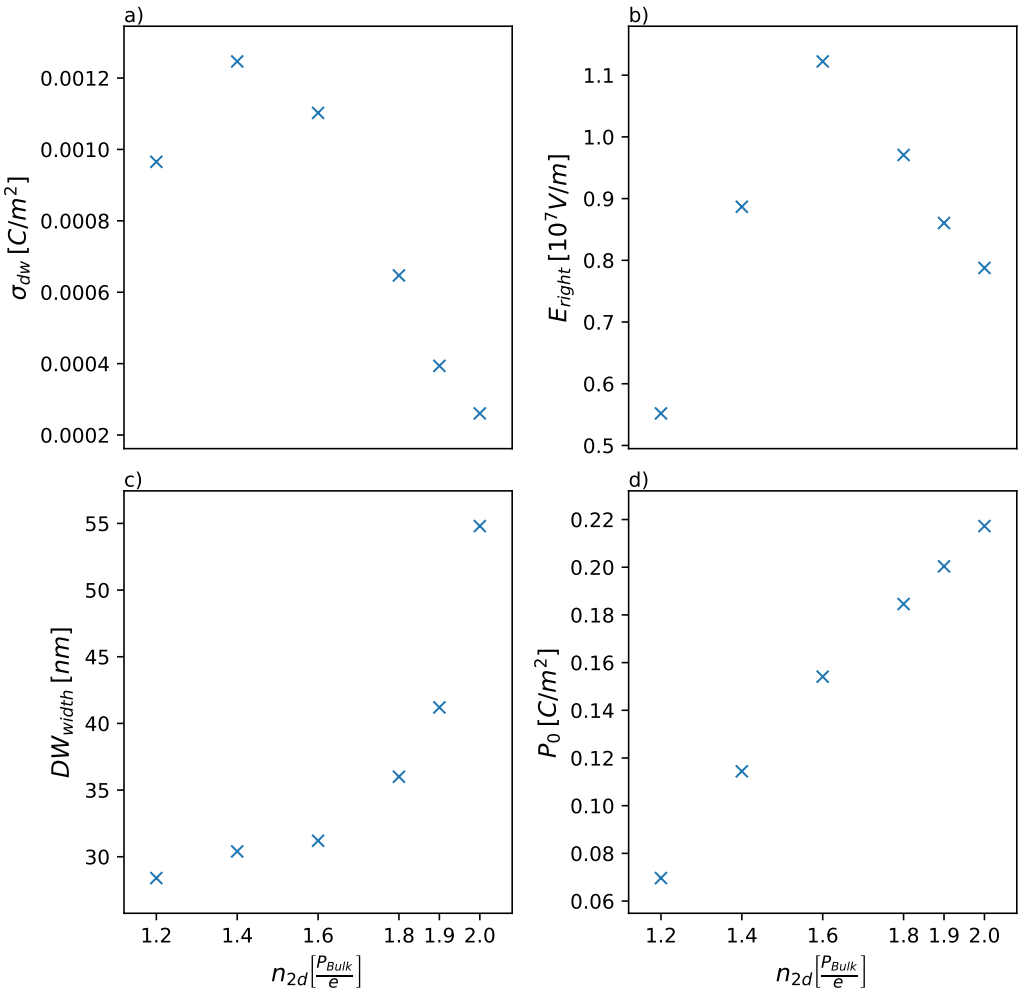

Figure 4.13: (a) σ_{dw} vs n_{2d}. (b) E_{right} vs n_{2d}. The change in the electric field away from the DW. (c) DW_{width} vs n_{2d}. (d) P_0 vs n_{2d}. All at $\Delta V = 1V$

electric field might decrease as a whole and shift left, or increase as a whole and not shift, which translates into the non-smooth curve seen in panel b).

Lastly, we look at the DW displacement, DW charge, and E_{right}, going from $\Delta V = 0V$ to $\Delta V = 1V$ as a function of n_{2d}. In panel a) we see how far the center of the DW moves when a bias voltage is applied for each n_{2d} value. For the largest three n_{2d} values Δz is negligible, and then it changes linearly with n_{2d}. In panel b) we see the change in the DW charge. For the first two n_{2d} values we see that $\Delta\sigma_{DW}$ is negative, meaning the DW

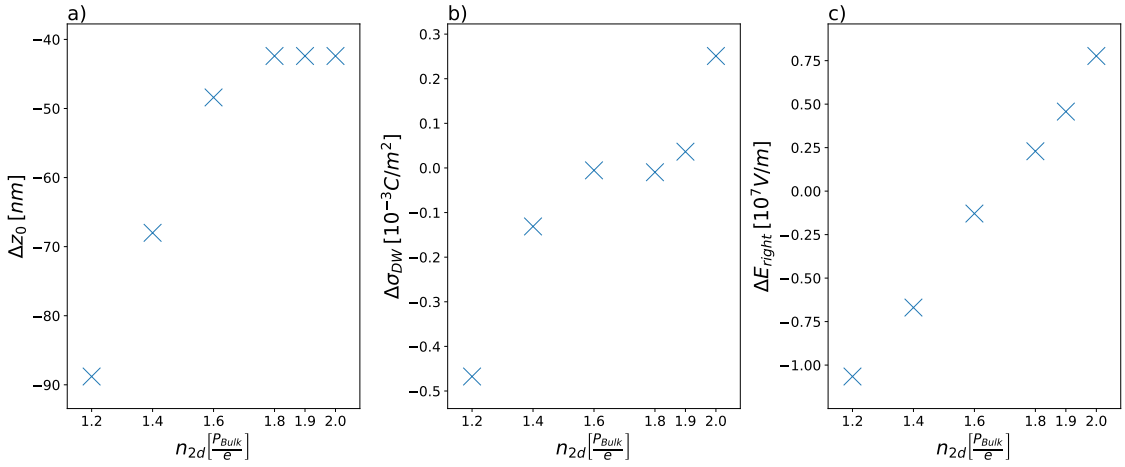

Figure 4.14: (a) The shift in DW position when a bias voltage $\Delta V = 1$, is applied. (b) The change in the DW charge σ_{dw} when a bias voltage is applied. (c) The change in the electric field away from the DW when a bias voltage is applied.

becomes more negatively charged when a bias voltage is applied. The next two n_{2d} values we see $\Delta\sigma_{DW} \approx 0$. The last two n_{2d} values we see that $\Delta\sigma_{DW}$ is positive, meaning the DW becomes more positively charged when a bias voltage is applied. In panel c) we see the change in E_{right} as a bias voltage is applied. Interestingly we see a very linear change as n_{2d} increases, starting from a negative ΔE_{right} to a positive ΔE_{right}.

Fig. 4.12 - Fig. 4.14 highlight the key measurable quantities from Section 4.2 and 4.2 and how they change when a bias voltage is applied for varying n_{2d}. This allows us to get a better understanding of what happens when we go beyond Sturman's assumptions. The main thing that we see is that a bias voltage will move the DW. We also see that a bias voltage affects the DW charge and electric field, and affects these two quantities differently depending on n_{2d}. The calculations until now were done for a system with $L = 200nm$ which was used to represent a infinite system when $\Delta V = 0$. Next, we are going to go beyond the assumption that the system has an infinite length and look at two systems with $L = 10nm$ and $L = 5nm$.

Size Effects

In the final subsection of results we are going to go beyond Sturman's assumption of an infinite system length and look at size effects. Previously, we have been using a system with

$L = 200nm$, which was chosen to represent an infinite system size when $\Delta V = 0$. However, thin-film ferroelectrics are a topic of interest [33]. Thin-film ferroelectrics were thought to have suppressed polarization due to size effects, but with sufficient screening charge, like in the case of a charged domain wall, the polarization can persist [34, 35]. Experimental work on CDWs and writable electronics have been looking at system sizes ranging from approximately $2nm - 20nm$ [8, 9]. $BaTiO_3$ has been shown to have a critical thickness, meaning the minimum thickness of the sample at which there is a spontaneous polarization, of 5nm [36]. Taking into consideration the critical thickness of $BaTiO_3$ and the system sizes of experimental work, we will be look at two systems with $L = 10nm$ and $L = 5nm$. We will then be varying n_{2d} and ΔV to see how polarization, electric field, electron density, and DW charge is affected.

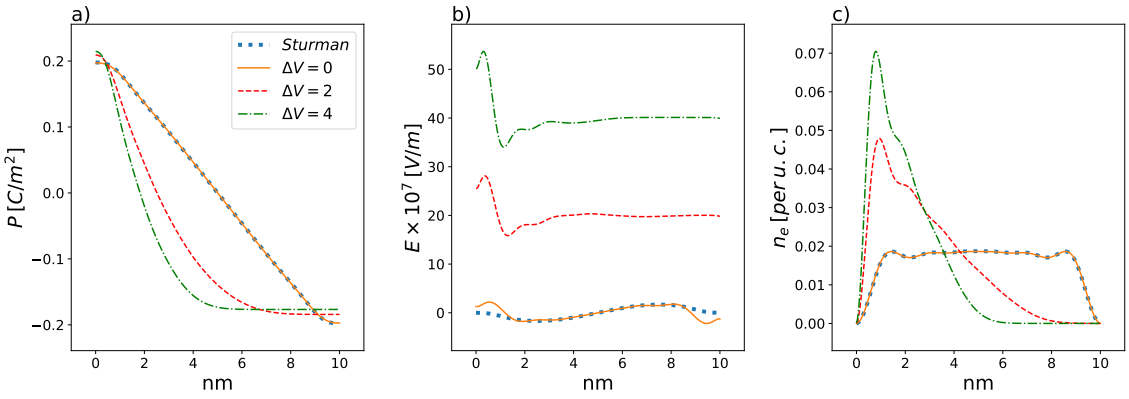

Figure 4.15: Polarization, electric field, and electron density for $BaTiO_3$ parameters with $n_{2d} = 2\frac{P_{Bulk}}{e}$, $L = 10nm$, $\Delta V = 0V$, $2V$, and $4V$, and a solution using Sturman's approximations labelled 'Sturman'. (a) depicts the polarization profiles corresponding for each value of the bias voltage. (b) depicts the electric field profiles. (c) depicts the electron density profiles.

Figure 4.15 and 4.16 show the polarization, electric field, and electron density profiles for a $10nm$ sample size of $BaTiO_3$ for various bias voltages when $n_{2d} = 2\frac{P_{Bulk}}{e}$ and $1.2\frac{P_{Bulk}}{e}$, respectively. The first thing to note is that the polarization profiles have a much different shape, when compared with the $200nm$ system, and do not resemble the tanh solution for an infinite system. The system size is now on the scale of the DW width so the polarization is not able to saturate like it did when $L = 200nm$. We also do not see a significant decrease in the polarization due to the size of the system, just a decrease in polarization as the n_{2d}

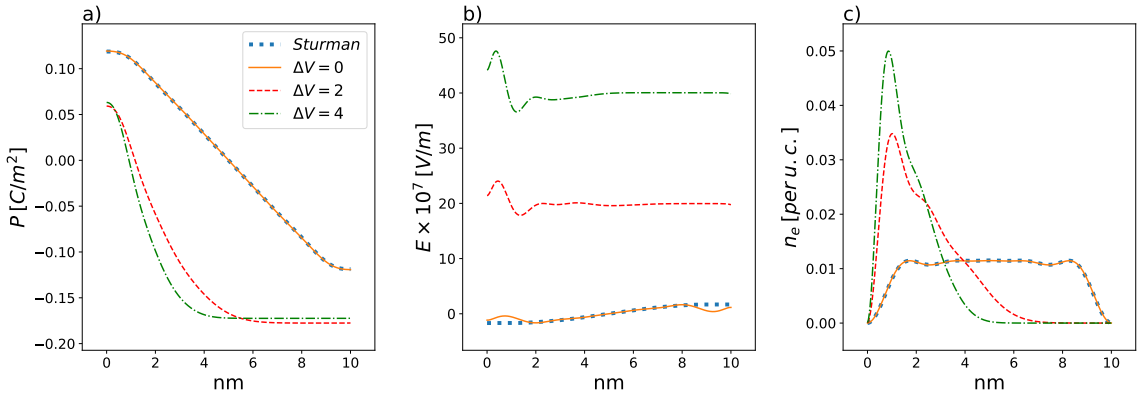

Figure 4.16: Polarization, electric field, and electron density for $BaTiO_3$ parameters with $n_{2d} = 1.2\frac{P_{Bulk}}{e}$, $L = 10nm$, $\Delta V = 0V$, $2V$, and $4V$, and a solution using Sturman's approximations labelled 'Sturman'. (a) depicts the polarization profiles corresponding for each value of the bias voltage. (b) depicts the electric field profiles. (c) depicts the electron density profiles.

value is lowered. For $\Delta V = 0$ we see that the approximated solution labelled 'Sturman' is nearly identical to the exact numerical solution for each quantity.

When we apply a large enough bias voltage we are able to manipulate the DW considerably, moving the DW roughly $2.5nm$. Note that the center of the DW is defined to be where $P = 0$. The DW width in this case is a bit harder to resolve as the profile is asymmetric. One can look at the electron density profile to get a better idea of the DW width. Where the electron density approaches zero is an indication of the DW boundaries. We see the DW width get smaller as the bias voltage increases. We also see a large migration of electrons due to the bias voltage, increasing the peak density by over a factor of 3.

Figure 4.17 and 4.18 show the polarization, electric field, and electron density profiles for a 5nm sample size of $BaTiO_3$ for various bias voltages when $n_{2d} = 2\frac{P_{Bulk}}{e}$ and $1.2\frac{P_{Bulk}}{e}$, respectively. We see a similar polarization profile as the 10nm sample, but less DW movement. As a whole there does not seem to be much difference in a 5nm and 10nm system size. We see a smaller shift in the DW position and electron density peak due to boundary restrictions in the 5nm sample. For the cases of $1.2\frac{P_{Bulk}}{e}$ and both system sizes, we see that the applied bias voltage has an interesting affect. One might expect the external electric field to enhance the region of positive polarization and decrease the region of negative polarization, as the electric field is pointing towards the right. We see the opposite effect,

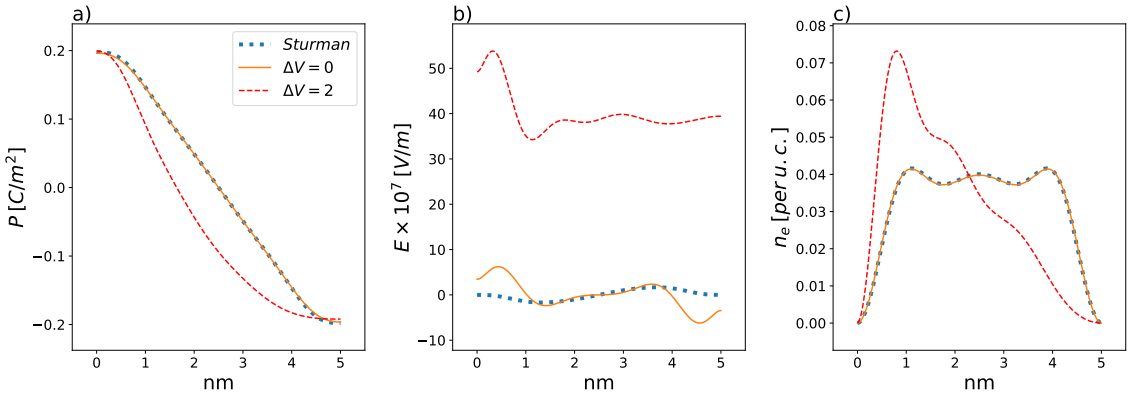

Figure 4.17: Polarization, electric field, and electron density for a $BaTiO_3$ sample with $n_{2d} = 2\frac{P_{Bulk}}{e}$, $L = 5nm$, and a bias voltage of 0V and 2V(a) depicts the polarization profiles corresponding for each value of the bias voltage.(b) depicts the electric field profiles.(c) depicts the electron density profiles.

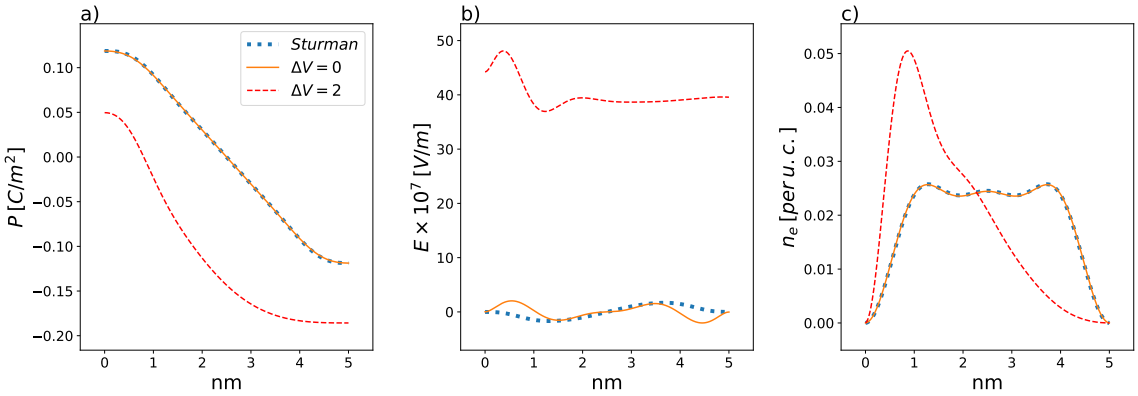

Figure 4.18: Polarization, electric field, and electron density for a $BaTiO_3$ sample with $n_{2d} = 1.2\frac{P_{Bulk}}{e}$, $L = 5nm$, and a bias voltage of 0V and 2V(a) depicts the polarization profiles corresponding for each value of the bias voltage.(b) depicts the electric field profiles.(c) depicts the electron density profiles.

however. The DW is moving to the left and the negative region of polarization becomes larger and the polarization becomes more negative. It is assumed that this is happening because it is lowering the free energy. The polarization is approaching its bulk value in the negative region, which is the solution for the lowest free energy.

One difference in a system size of $200nm$ and $10nm/5nm$ is the charge on the DW. The DW charge values are presented in Table 4.3 and 4.4. For $n_{2d} = 2\frac{P_{Bulk}}{e}$, the $10nm$ system has a negatively charged DW while the $200nm$ system had a positively charged DW. For $n_{2d} = 1.2\frac{P_{Bulk}}{e}$, the $10nm$ system has a positively charged DW that becomes negatively

σ_{DW}	$n_{2d} = 2.0\frac{P_{Bulk}}{e}$	1.2
$\Delta V = 0$	$-1.13[\cdot 10^{-3}\, C/m^2]$	1.02
$\Delta V = 2$	$-2.53[\cdot 10^{-3}\, C/m^2]$	-0.74
$\Delta V = 4$	$-4.53[\cdot 10^{-3}\, C/m^2]$	-1.92

Table 4.3: DW Charge for L = 10nm

σ_{DW}	$n_{2d} = 2.0\frac{P_{Bulk}}{e}$	1.2
$\Delta V = 0$	$-3.07[\cdot 10^{-3}\, C/m^2]$	-0.02
$\Delta V = 2$	$-4.36[\cdot 10^{-3}\, C/m^2]$	-2.07

Table 4.4: DW Charge for L = 5nm

charged when a bias voltage is applied. The $5nm$ has a negatively charged DW for all n_{2d} and becomes more negatively charged when a bias voltage is applied. However, in all cases the DW moves against the electric field, to the left. One could expect negatively and positively CDWs to move in opposite directions.

4.3 Discussion

4.3.1 Approximations

In Sec. 4.1 we looked at how well the approximations of Sturman *et al.* do for two theoretical parameter sets. We see that overall the approximations do quite well within the limitations, and do slightly better for one parameter set compared to the other. When we disregard the gradient term in the LGD equation we see the biggest difference when compared with the exact numerical solution. Disregarding the electric field term in Gauss's law doesn't have as big of an impact on the solution. This approximation, however, significantly reduces the calculation run time, approximately 10-fold. The 1-D problem we are solving takes a few hours to run when we solve for the exact numerical solutions, depending on the parameters. A more complex geometry such as a 2-D problem, could take many hours or even on the order of days. The idea would be to apply these approximations to complex problems, speeding up the run time significantly, while still giving accurate results. Within the limitations the approximations this would give reliable results.

4.3.2 Universal CDW

In Sec. 4.2 we focused on one material, $BaTiO_3$, since this a highly studied material and has been shown to have a 90 degree H-T-H CDW [13,19,37,38]. We showed that Sturman's approximations do quite well for most n_{2d} values, but break down for low n_{2d}. Since his equations are not set up to include a bias voltage we were only able to compare with our method for $\Delta V = 0V$. Next we looked at the properties of a CDW for varying n_{2d} values at $\Delta V = 1V$, to see how a bias voltage affects things. Since thin-film ferroelectrics are of interest we decided to look at size effects on a CDW at different bias voltages and varying n_{2d}.

Starting with Sec. 4.2. Here we showed what happens to the polarization, electric field, and electron density when n_{2d} is varied. We then compared the exact numerical solutions to solutions using Sturman's approximations that go beyond the assumption that there is as much free charge as bound charge. We see that for larger n_{2d} values the approximations do well. As n_{2d} is lowered we start to see a small difference in the exact numerical solutions and the solutions using Sturman's approximations. Realistically, there would not be as much free charge as bound charge, meaning that the cases of low n_{2d} are more representative of real materials. The approximated solutions are less reliable at low n_{2d}, but still do a good job. The approximation that $\rho_b = -\rho_f$, which leads to the assumption that there is as much free charge as bound, is the approximation that speeds up the calculation time significantly. So, one would have to weigh out if the accuracy of the calculations or run time is more important. However, this approximation also does not let one apply a bias voltage to the system.

In Sec. 4.2 we go beyond the assumption of no bias voltage. Here we looked at the affect of a bias voltage with varying n_{2d}, but we were not able to compare with solutions using Sturman's approximations since his approximations do not allow for a bias voltage. We see that a bias voltage will move the DW and depending on n_{2d} the DW will move a different amount of distance for the same ΔV. We also show that the DW is positively charged and when a bias voltage is applied becomes more positively charged for large n_{2d} and less positively charged for low n_{2d}. While the DW is positively charged in all cases, it moved

against the direction of the electric field. One could expect the positively charged DW to repel the electric field and move with the field (towards the negative end). Chapman *et al.* also found the same kind of DW displacement for a positively charged DW [27]. However, the model in Chapman *et al.* differs from the model used in this thesis. Chapman *et al.* is looking at the interface of a dielectric and ferroelectric material where the left bound is the interface and everything to the right is a ferroelectric material. all three orbitals

Finally, in Sec. 4.2 we go beyond the assumption of an infinite film thickness. Here we looked at the effect of shrinking the system size, we took two system sizes of $L = 10nm$ and $L = 5nm$. The first thing we see is that the polarization profile no longer takes on the $tanh$ solution when $L = 200nm$. However, the approximated solution is nearly identical to the exact numerical solution for $\Delta V = 0$ and for each n_{2d}. We can say the approximations give reliable results when we go beyond an infinite system and vary n_{2d} for $\Delta V = 0$.

Next we see that the DW and the electron density distribution now spans the length of the system for $\Delta V = 0$. This leads to a negatively charged DW for $n_{2d} = 2\frac{P_{Bulk}}{e}$ and becomes more negatively charged when we apply a bias voltage. For $n_{2d} = 1.2\frac{P_{Bulk}}{e}$ we find a positively charged DW which becomes negatively charged when we apply a bias voltage. Regardless of the charge sign on the DW, the DW still moves against the external electric field. This behaviour is not what is expected, it was thought that a positively charged DW and a negatively charged DW would move in opposite directions.

We can compare our results of a small sample size to experimental data from Liu *et al.* [9]. This experimental work looks at a CDW with a T-T-T configuration in a $BiFeO_3$ thin-film when a bias voltage is applied. Their sample size is roughly 2-3 nm in length which is smaller when compared with our sample size of 5 nm and 10 nm. It is not shown in the data what the net charge on the DW is, but one can assume a negatively charged DW as it is a T-T-T configuration (the negative bound charge is lined up at the DW). The screening charge comes from oxygen vacancies to stabilize the DW. This system configuration is the counterpart to what we are interested in. They show that the CDW moves against the direction of the external electric field. If the net charge is indeed negatively charged, then this DW movement would be expected. The results we show for a small sample size (5 nm and 10 nm) and a negatively charged DW would agree with this experiment. For our

results when $L = 200$nm we see the DW has a net positive charge and still moves in the same direction.

The question of "why does the DW move the way it does?" is still unanswered. We can shed a bit of light on the question by looking at the equation for the pressure on a DW (Eq.1.3) proposed by Gureev *et al* [26]. This equation doesn't tell us the 'why' but it tells us that our results for when a bias voltage is applied put the system in a lower free energy state. If we calculate the pressure when the domain wall is in the center position, we get a slight positive pressure. This slight positive pressure is expected as the positively charged DW would want to move with the electric field. When we calculate the pressure once the CDW has moved, which we see it move to the left, the pressure is now greatly negative. This suggests that once the CDW has moved it wants to continue moving in that direction. The first term in the equation is the difference in free energy on either side of the DW. We see this term become the dominant term once the DW has started to move. We can also see that the free energy of the domain that grows in size, from the DW moving, continues to lower the more the DW moves. What we can conclude from this equation is that our system is in an energetically favorable state, even if the DW movement is not what is expected.

Overall Sturman's approximations work well when $\Delta V = 0$, even when we go beyond the limitations. While the approximated solutions are not exactly the same as the exact numerical solutions, the difference in run time is significant enough to look past a small margin of error. The biggest problem with the approximated method is the inability to apply a bias voltage. Future work could look into constructing equations that allow for a bias voltage using the approximations of Sturman *et al*.

A question that still goes unanswered is, why does the DW move the way it does? We see that the DW displacement is different for each n_{2d} while ΔV is held constant. We also see that regardless of the DW charge, the DW moves in the same direction when a bias voltage is applied. This would suggest there is more going on at the DW, and one can not simply look at the sign of the DW charge. We also know that whether the DW moves in an expected way or not, it is in an energetically favorable position.

Chapter 5

Conclusion

Previously the domains that form in ferroelectric materials were considered for their electrical, electromechanical, and optical properties. Recently, domain walls are being considered for their re-configurable conductive properties, specifically charged domain walls which get their conductive properties from a H-T-H polarization configuration. The bound charge at the domain wall will attract free electrons and they will act as a conducting channel. The conducting channel is re-configurable by an external electric field. This opens the doors for applications of re-configurable nano-circuitry.

We looked to build an efficient model to describe the properties of charged domain walls. The model self-consistently solves Landau-Ginsburg-Devonshire theory to describe the polarization, Guass's law to describe the electric field and electric potential, and a discrete Schrodinger's equation to describe the free electrons (amount of electrons is given by two dimensional electron density, n_{2d}). It takes a significant amount of time to computationally solve these equations. Sturman *et al.* have proposed a set of equations that suggest a universal form for charged domain walls. These equations use approximations which speed up the calculation time 10-fold. We compared exact numerical solutions with solutions using Sturman's approximations. We found that for two sets of theoretical parameters the approximations produce very similar solutions when compared with the exact solutions.

Sturman *et al.* is not the only work to suggest a universal picture for charged domain walls. Charged domain walls are often depicted with infinite film thickness, being charge neutral, and no bias voltage applied. Experimental work, however, goes beyond these

assumptions. CDWs are produced with finite film thickness (thin-film or ultra thin-film), the CDW is not charge neutral, and a bias voltage is being applied as it is the main mechanism for their desired property.

We started with the assumption that the DW is charge neutral. In practice it is unlikely that the free charge and bound charge are equal. To go beyond this assumption we looked at the polarization, electric field, and electron density for varying n_{2d}. We find that the approximations do quite well, with a slight difference in solutions for low n_{2d}. The polarization was shown to decrease with n_{2d} as there is less electrons to screen the bound charge, leading to a larger depolarizing field. The universal polarization profile started to breakdown for low n_{2d}.

The next assumption is that there is no bias voltage. The approximated equations of Sturman *et al.* are not set up to apply a bias voltage. So, we looked at the effect of a bias voltage on a CDW for varying n_{2d} values, without comparing to the approximated solutions. The CDW was found to be positively charged and moved against the direction of the external electric field. This results was not expected, as the positively charged DW would repel the electric field. However, this was also seen in Chapman *et al.* [27]. Depending on n_{2d} the CDW displacement was different. The exact mechanism as to why it moves the way it does is unclear, but clearly influenced by the n_{2d} value.

Lastly, we went beyond the assumption of a infinite system size. We scaled our system down from 200 nm to 10 nm and 5 nm to see the effects of different n_{2d} values and a bias voltage on a small sample size. $BaTiO_3$ has been shown to have a critical thickness of 5 nm, which is the reason for the system sizes. For $\Delta V = 0$ we found that Sturman's approximations do very well, producing nearly identical results to the exact numerical solutions. For $\Delta V > 0$ we could not compare our exact numerical solutions to approximated solutions. We found that the DW essentially spans the length of the system for $\Delta V = 0$ with an even distribution of electrons. Once the bias voltage was increased we saw significant movement in the DW and a reduction in DW width. The electron density migrated due to the attraction of the external electric field creating a large peak in the density. The DW is negatively charged for large n_{2d} and positively charged for low n_{2d}, and when a bias voltage was applied we saw that the net charge on the DW was negative for both sample sizes. The

DWs moved in the same direction for both sample sizes, to the left. In all of our results we found the DW moved against the external electric field, regardless of DW charge. This would suggest there is more going on at the DW, and one can not simply look at the sign of the DW charge.

Overall Sturman's approximations work well when $\Delta V = 0$, even when we go beyond the limitations. While the approximated solutions are not exactly the same as the exact numerical solutions, the difference in run time is significant enough to look past a small margin of error. The biggest problem with the approximated method is the inability to apply a bias voltage. When we went beyond the assumptions for a universal CDW we see a complete breakdown in the picture of a universal CDW. We were left with unanswered questions regarding why we see the behaviour we do.

5.1 Future Work

Here we discuss future work that could be done to better answer the questions we set out for this thesis. The main question that needs to be answered is why does the DW move the way it does? The charge on the DW seems to have no affect on the displacement direction and the value of n_{2d} determines how far it moves, but why?

The first thing to do would be to compare these results with other material parameters. Do weakly or strongly polarized materials respond differently?

Similar to how we compared the results with Chapman *et al.*, another step in attempting to answering the objective questions would be to directly compare results with someone elses model. For example a fellow graduate student was looking at the formation of 2D zigzag CDWs. If we used the same parameters would we see similar behaviour when there is more degrees of freedom? Do they move in the same direction?

One could also consider creating a toy model. This would be a stripped down version of method and model in this thesis that would be easier to analyze. Each parameter could be varied one at a time to get a better understanding of what is happening and the main properties could be calculated much faster. It could show qualitatively the same behaviour without some of the details.

Bibliography

[1] Urko Petralanda, Mads Kruse, Hugh Simons, and Thomas Olsen. Oxygen vacancies nucleate charged domain walls in ferroelectrics. *Phys. Rev. Lett.*, 127:117601, Sep 2021.

[2] Hemaprabha Elangovan, Maya Barzilay, Jiawei Huang, Shi Liu, Shai Cohen, and Yachin Ivry. Engineering individual oxygen vacancies: Domain-wall conductivity and controllable topological solitons. *ACS Nano*, 15(8):13380–13388, 2021. PMID: 34355902.

[3] Xian-Kui Wei, Tomas Sluka, Barbara Fraygola, Ludwig Feigl, Hongchu Du, Lei Jin, Chun Lin Jia, and Nava Settert. Controlled charging of ferroelastic domain walls in oxide ferroelectrics. *ACS APPLIED MATERIALS & INTERFACES*, 9(7):6539–6546, FEB 22 2017.

[4] B. Sturman, E. Podivilov, M. Stepanov, A. Tagantsev, and N. Setter. Quantum properties of charged ferroelectric domain walls. *Physical Review B*, 92(21):214112, Dec 2015.

[5] Karin M. Rabe, Chong H. Ahn, and Jean-Marc Triscone. *Physics of Ferroelectrics : A Modern Perspective*. Springer, Jan 2007.

[6] JF Scott and CAP Desraujo. Ferroelectric memories. *Science*, 246(4936):1400–1405, DEC 15 1989.

[7] Pankaj Sharma, Qi Zhang, Daniel Sando, Chi Hou Lei, Yunya Liu, Jiangyu Li, Valanoor Nagarajan, and Jan Seidel. Nonvolatile ferroelectric domain wall memory. *Science Advances*, 3(6), JUN 2017.

[8] Linze Li, Jason Britson, Jacob R. Jokisaari, Yi Zhang, Carolina Adamo, Alexander Melville, Darrell G. Schlom, Long-Qing Chen, and Xiaoqing Pan. Giant resistive switching via control of ferroelectric charged domain walls. *Advanced Materials*, 28(31):6574+, AUG 17 2016.

[9] Zhongran Liu, Han Wang, Ming Li, Lingling Tao, Tula R. Paudel, Hongyang Yu, Yuxuan Wang, Siyuan Hong, Meng Zhang, Zhaohui Ren, Yanwu Xie, Evgeny Y. Tsymbal, Jingsheng Chen, Ze Zhang, and He Tian. In-plane charged domain walls with memristive behaviour in a ferroelectric film. *Nature*, 613(7945):656+, JAN 26 2023.

[10] Ca Randall, Dj Barber, and Rw Whatmore. Ferroelectric domain configurations in a modified-pzt ceramic. *Journal of Materials Science*, 22(3):925–931, MAR 1987.

[11] PJ Lin and LA Bursill. On the width of charged (110) ferroelectric domain-walls in potassium niobate. *Philosphical Magazine A-Physics of Condensed Matter Structure Defects and Machanical Properties*, 48(2):251–263, 1983.

[12] Chun-Lin Jia, Shao-Bo Mi, Knut Urban, Ionela Vrejoiu, Marin Alexe, and Dietrich Hesse. Atomic-scale study of electric dipoles near charged and uncharged domain walls in ferroelectric films. *Nature Materials*, 7(1):57–61, December 2007.

[13] Tomas Sluka, Alexander K. Tagantsev, Petr Bednyakov, and Nava Setter. Free-electron gas at charged domain walls in insulating batio¡sub¿3¡/sub¿. *Nature Communications*, 4, MAY 2013.

[14] Christoph S. Werner, Simon J. Herr, Karsten Buse, Boris Sturman, Elisabeth Soergel, Cina Razzaghi, and Ingo Breunig. Large and accessible conductivity of charged domain walls in lithium niobate. *Scientific Reports*, 7(1):9862, August 2017.

[15] Eugene A. Eliseev, Anna N. Morozovska, George S. Svechnikov, Peter Maksymovych, and Sergei V. Kalinin. Domain wall conduction in multiaxial ferroelectrics. *Physical Review B*, 85(4):045312, Jan 2012.

[16] Peter Maksymovych, Anna N. Morozovska, Pu Yu, Eugene A. Eliseev, Ying-Hao Chu, Ramamoorthy Ramesh, Arthur P. Baddorf, and Sergei V. Kalinin. Tunable metallic conductance in ferroelectric nanodomains. *Nano Letters*, 12(1):209–213, JAN 2012.

[17] Kalani Moore, Michele Conroy, Eoghan N. O'Connell, Charlotte Cochard, Jennifer Mackel, Alan Harvey, Thomas E. Hooper, Andrew J. Bell, J. Marty Gregg, and Ursel Bangert. Highly charged 180 degree head-to-head domain walls in lead titanate. *COMMUNICATIONS PHYSICS*, 3(1), DEC 15 2020.

[18] G. F. Nataf, M. Guennou, J. M. Gregg, D. Meier, J. Hlinka, E. K. H. Salje, and J. Kreisel. Domain-wall engineering and topological defects in ferroelectric and ferroelastic materials. *NATURE REVIEWS PHYSICS*, 2(11):634–648, NOV 2020.

[19] Qianwei Huang, Jiyuan Yang, Zibin Chen, Yujie Chen, Matthew J. Cabral, Haosu Luo, Fei Li, Shujun Zhang, Yulan Li, Zonghan Xie, Houbing Huang, Yiu-Wing Mai, Simon P. Ringer, Shi Liu, and Xiaozhou Liao. Formation of head/tail-to-body charged domain walls by mechanical stress. *ACS Applied Materials & Interfaces*, 2022 DEC 19 2022.

[20] T Denneulin and A S Everhardt. A transmission electron microscopy study of low-strain epitaxial $BaTiO_3$ grown onto $NdScO_3$. *Journal of Physics: Condensed Matter*, 34(23):235701, June 2022.

[21] Felix Risch, Yuri Tikhonov, Igor Lukyanchuk, Adrian M. Ionescu, and Igor Stolichnov. Giant switchable non thermally-activated conduction in 180° domain walls in tetragonal $Pb(Zr, Ti)O_3$. *Nature Communications*, 13(1):7239, November 2022.

[22] James P. V. McConville, Haidong Lu, Bo Wang, Yueze Tan, Charlotte Cochard, Michele Conroy, Kalani Moore, Alan Harvey, Ursel Bangert, Long-Qing Chen, Alexei Gruverman, and J. Marty Gregg. Ferroelectric Domain Wall Memristor. *Advanced Functional Materials*, 30(28):2000109, July 2020.

[23] Petr S. Bednyakov, Boris I. Sturman, Tomas Sluka, Alexander K. Tagantsev, and Petr V. Yudin. Physics and applications of charged domain walls. *npj Computational Materials*, 4(1), 2018.

[24] I. Luk'yanchuk, A. Sené, and V. M. Vinokur. Electrodynamics of ferroelectric films with negative capacitance. *Physical Review B*, 98(2):024107, Jul 2018.

[25] M Y Gureev, A K Tagantsev, and N Setter. Head-to-head and tail-to-tail 180○ domain walls in an isolated ferroelectric. *Physical Review B*, 83:184104, 2011.

[26] M. Y. Gureev, P. Mokrý, A. K. Tagantsev, and N. Setter. Ferroelectric charged domain walls in an applied electric field. *Physical Review B*, 86(10):104104, Sep 2012.

[27] Kelsey S. Chapman and W. A. Atkinson. Mechanism for switchability in electron-doped ferroelectric interfaces. *Physical Review B*, 105(3), jan 2022.

[28] A. P. Levanyuk, B. A. Strukov, and A. Cano. Background dielectric permittivity: Material constant or fitting parameter? *Ferroelectrics*, 503(1, SI):94–103, 2016.

[29] JM Neuberger, DR Rice, and JW Swift. Numerical solutions of a vector ginzburg-landau equation with a triple-well potential. *International Journal of Bifurcation and Chaos*, 13(11):3295–3306, NOV 2003.

[30] Donald G. M. Anderson. Comments on "anderson acceleration, mixing and extrapolation". *Numerical Algorithms*, 80(1):135–234, JAN 2019.

[31] Yao Tian, Carolina Adamo, Darrell G Schlom, and Kenneth S Burch. Optical properties of srtio3 on silicon (100). *Applied Physics Letters*, 102(4), 2013.

[32] J. J. Wang, F. Y. Meng, X. Q. Ma, M. X. Xu, and L. Q. Chen. Lattice, elastic, polarization, and electrostrictive properties of batio¡sub¿3¡/sub¿ from first-principles. *JOURNAL OF APPLIED PHYSICS*, 108(3), AUG 1 2010.

[33] Abel Fernandez, Megha Acharya, Han-Gyeol Lee, Jesse Schimpf, Yizhe Jiang, Djamila Lou, Zishen Tian, and Lane W. Martin. Thin-film ferroelectrics. *Advanced Materials*, 34(30), JUL 2022.

[34] W. L. Zhong, Y. G. Wang, P. L. Zhang, and B. D. Qu. Phenomenological study of the size effect on phase transitions in ferroelectric particles. *Phys. Rev. B*, 50:698–703, Jul 1994.

[35] S Li, JA Eastman, JM Vetrone, CM Foster, RE Newnham, and LE Cross. Dimension and size effects in ferroelectrics. *Japanese Journal of Applied Physics*, 36(8):5169–5174, AUG 1997.

[36] YS Kim, DH Kim, JD Kim, YJ Chang, TW Noh, JH Kong, K Char, YD Park, SD Bu, JG Yoon, and JS Chung. Critical thickness of ultrathin ferroelectric $BaTiO_3$ films -: art. no. 102907. *Applied Physics Letters*, 86(10), MAR 7 2005.

[37] Petr S. Bednyakov, Tomas Sluka, Alexander K. Tagantsev, Dragan Damjanovic, and Nava Setter. Formation of charged ferroelectric domain walls with controlled periodicity. *Scientific Reports*, 5(1):15819, October 2015.

[38] K. Yokoo H. Kakemoto S. Wada, K. Yako and T. Tsurumi. Domain wall engineering in barium titanate single crystals for enhanced piezoelectric properties. *Ferroelectrics*, 334(1):17–27, 2006.

Appendix A

$BaTiO_3$ L = 200nm

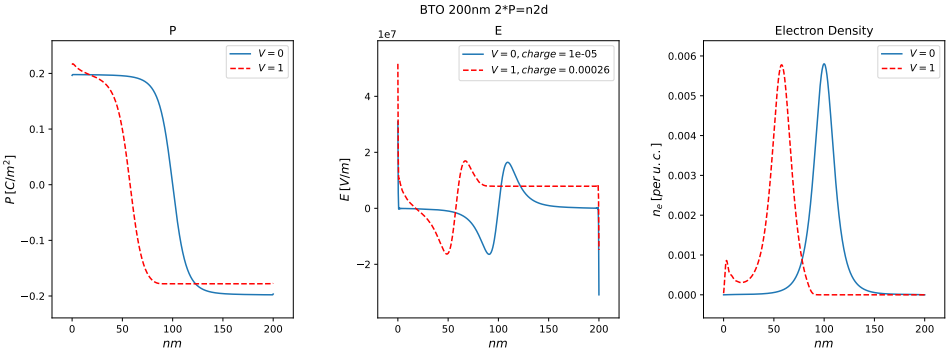

Figure A.1: Polarization, electric field, and electron density profiles for $n_{2d} = 2\frac{P_{Bulk}}{e}$ with and without a bias voltage.

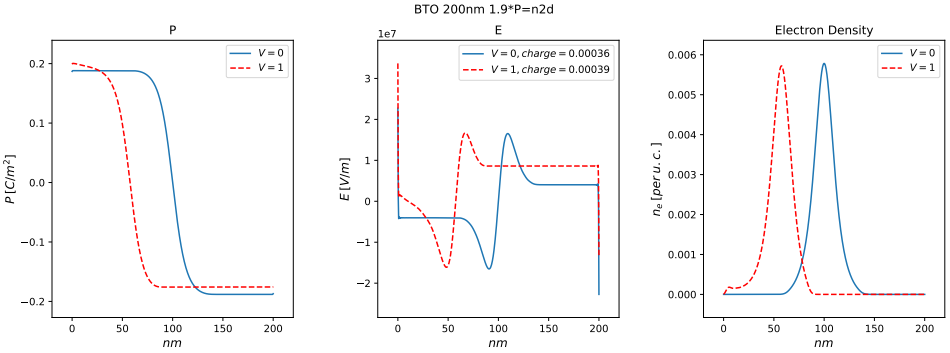

Figure A.2: Polarization, electric field, and electron density profiles for $n_{2d} = 1.9\frac{P_{Bulk}}{e}$ with and without a bias voltage.

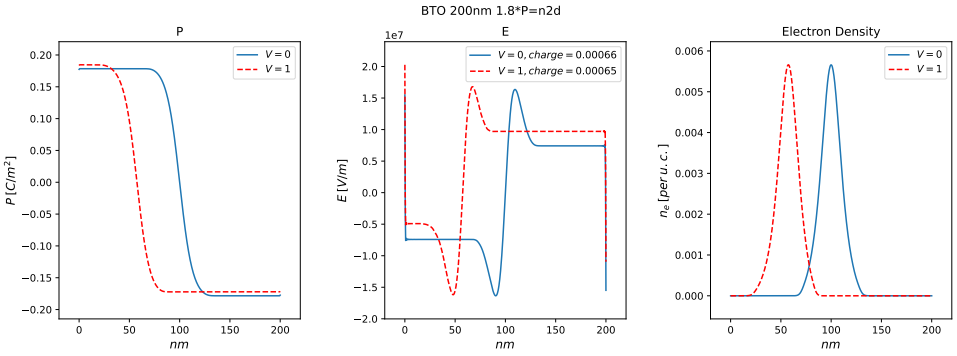

Figure A.3: Polarization, electric field, and electron density profiles for $n_{2d} = 1.8\frac{P_{Bulk}}{e}$ with and without a bias voltage.

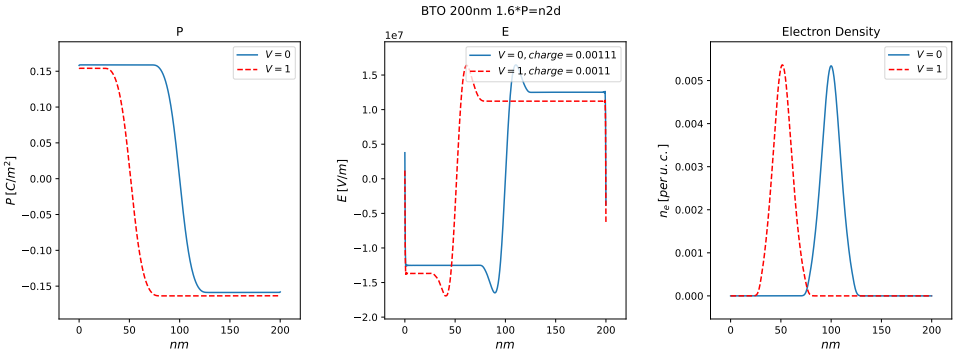

Figure A.4: Polarization, electric field, and electron density profiles for $n_{2d} = 1.6\frac{P_{Bulk}}{e}$ with and without a bias voltage.

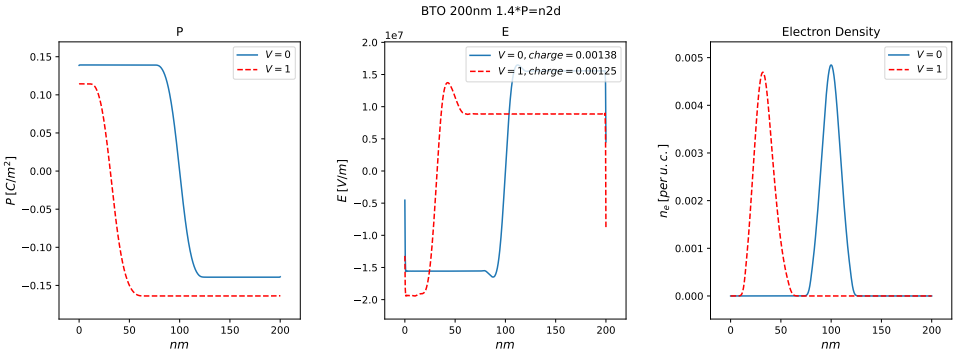

Figure A.5: Polarization, electric field, and electron density profiles for $n_{2d} = 1.4\frac{P_{Bulk}}{e}$ with and without a bias voltage.

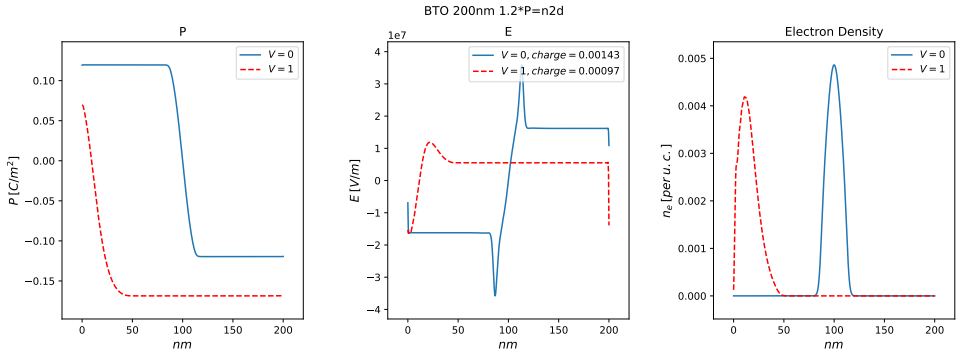

Figure A.6: Polarization, electric field, and electron density profiles for $n_{2d} = 1.2\frac{P_{Bulk}}{e}$ with and without a bias voltage.